Geochronologic Constraints on the Tectonic Evolution and Exhumation of Nanga Parbat, Western Himalaya Syntaxis, Revisited

D. A. Schneider,[1] P. K. Zeitler, W. S. F. Kidd,[2] and M. A. Edwards[3]

Department of Earth and Environmental Sciences, Lehigh University, Bethlehem, Pennsylvania 18015, U.S.A.

ABSTRACT

We examine the timing of deformation and exhumation of the Nanga Parbat-Haramosh massif in the western syntaxis of the Himalaya. This study presents geochronologic and thermochronologic data obtained from basement, shear zone, and intrusive units within the massif to reveal the Cenozoic tectonic evolution of the massif and to document the extent of the Plio-Pleistocene tectonic activity. These results combined with structural and petrologic observations indicate that the western Himalayan syntaxis was tectonically active for a protracted length of time and that the deformational succession was punctuated by three episodes since the beginning of the India-Asia collision: (1) The western syntaxial Indian plate rocks (future Nanga Parbat) underwent metamorphism, melting, and deformation during the initial collision of India with Asia and the associated island arc, the result of which is recorded as Eocene to Early Miocene metamorphic and magmatic ages and Oligocene cooling preserved in the Indian cover metasedimentary sequences that flank the younger, high-grade core. (2) Transpression along the South Karakorum fault to the north during the Late Miocene resulted in an episode of crustal scale doming and associated tectonometamorphic processes within the Himalaya syntaxis concurrent with the formation of other Late Miocene domes that developed in the Karakorum to the north and east. (3) At the core of the massif during the Plio-Pleistocene, the latest evolutionary stage of Nanga Parbat produced granulite-grade metamorphism, anatectic melting, and rapid cooling with deformation manifested as a pop-up structure, overprinting the Late Miocene doming.

Introduction

Orogenic belts commonly display locally exhumed high-grade rock termed "gneiss domes" or "metamorphic (core) complexes" that reflect a variety of tectonic settings (e.g., extension, compression, buoyancy-driven plutonism) (Getty and Gromet 1992; Amato et al. 1994). Such features are composed of metamorphic and plutonic rock that typically developed at amphibolite to granulite facies conditions during the latter stages of orogenesis. Genesis of these terranes appears to be intimately associated with thermal-magmatic events on the basis of spatial relationships between the high-grade metamorphic and plutonic rocks and adjacent granites and shear zones (e.g., Amato et al. 1994). However, despite the crucial nature of such information, in any high-grade terrane of such magmatic activity, information about the absolute timing of metamorphism or timing constraints on granite deformation is almost always lacking. In this article, we investigate the timing of magmatism, deformation, and accompanying exhumation of a large metamorphic complex in the Himalaya orogen, the Nanga Parbat-Haramosh massif (NPHM). Nanga Parbat is an especially notable case of recent, rapid exhumation because the petrologic and structural evolution of the massif may be genetically linked to the ferocious erosion and dynamic topography at the surface (Burbank et al. 1996; Koons and Zeitler 1997; Shroder and Bishop 1999; Zeitler et al. 2001). It is important to place the massif in a well-

Manuscript received September 12, 2000; accepted March 13, 2001.

[1] Current address: Department of Geological Sciences, Ohio University, Athens, Ohio 45701-2979, U.S.A.

[2] Department of Earth and Atmospheric Sciences, SUNY at Albany, Albany, New York 12222, U.S.A.

[3] Institut für Geologie, TU Bergakademie Freiberg, Berhard-von-Cotta Straße 2, D-09596 Freiberg, Germany.

[The Journal of Geology, 2001, volume 109, p. 563–583] © 2001 by The University of Chicago. All rights reserved. 0022-1376/2001/10905-0002$01.00

constrained geologic and geochronologic context before that discussion can be fully generated.

Nanga Parbat, situated at the well-accepted western terminus of the Himalayan chain (fig. 1), offers a unique opportunity to examine an unroofed, high-grade massif (Zeitler 1985) that is associated with recent magmatic activity (e.g., Schneider et al. 1999*c*). At Nanga Parbat, the Indian basement gneisses underwent Eocene high-grade metamorphism (Foster et al. 1999*b*, 2000) and Early Miocene

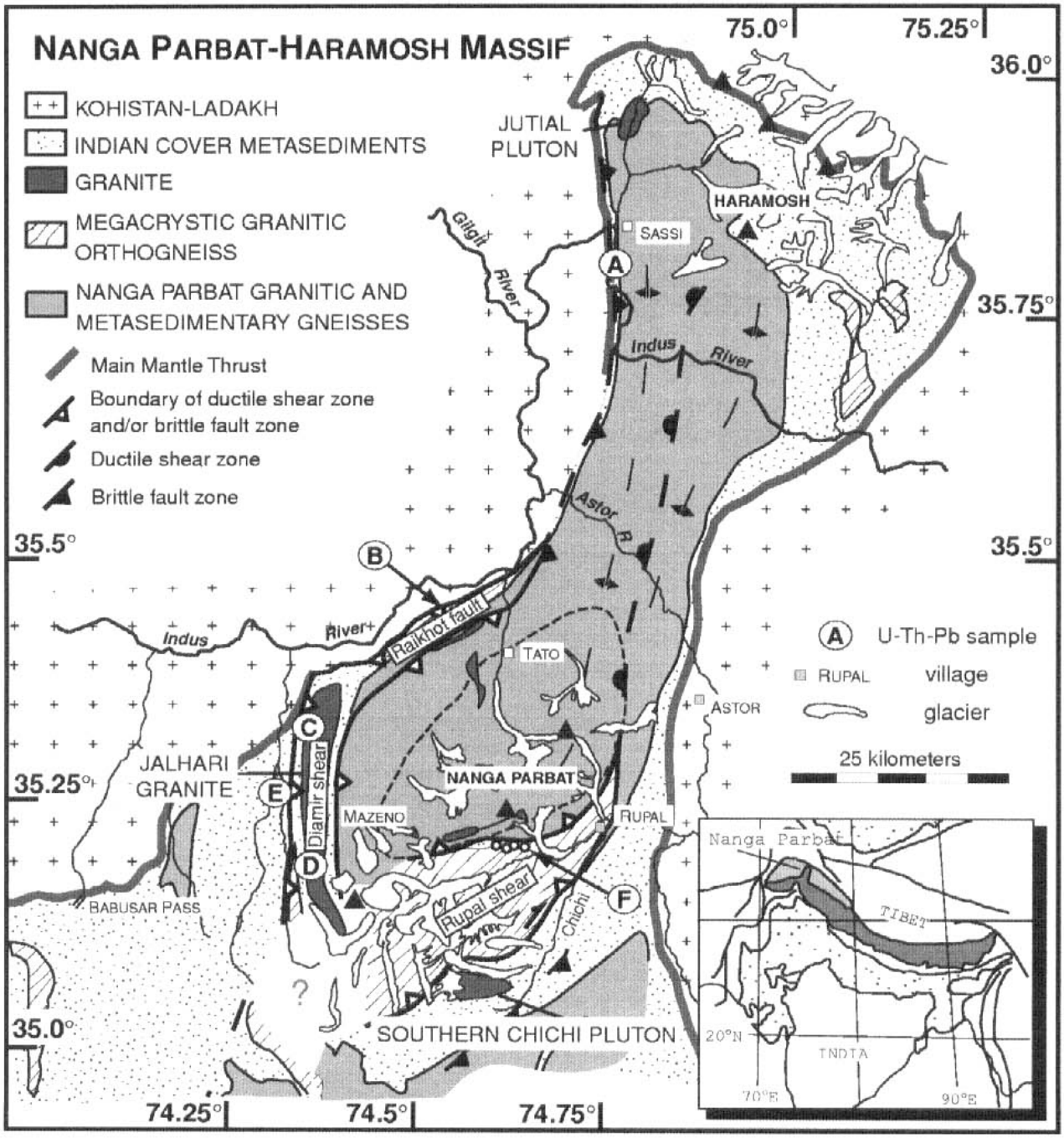

Figure 1. Geologic map of the Nanga Parbat massif (after Schneider et al. 1999*a*) showing locations of the granites and gneisses discussed in the text. *A*, IK-05; *B*, Jalipur augen gneiss at Patro Gah; *C*, Diamir section of Jalhari granite; *D*, Garal section of Jalhari granite; *E*, Manogush augen gneiss; *F*, Rupal leucogranite dikes. Dashed line near summit represents cordierite-K feldspar-sillimanite isograd. Solid triangles represent mountain summits.

anatexis (Schneider et al. 1999*b*) subsequently overprinted by Plio-Pleistocene high-grade metamorphism (Smith et al. 1992; Poage et al. 2000) and rapid exhumation and cooling (Zeitler 1985; Winslow et al. 1996). The latest anatectic event generated some of the youngest (1 Ma) syn- and postkinematic granites (Zeitler et al. 1993; Schneider et al. 1999*c*) yet reported for the Himalaya. Western Nanga Parbat continues to be active today, thrusting 1.8-Ga reworked gneisses over Quaternary glaciofluvial gravels. Here we present and discuss the tectonic significance of geochronologic constraints on basement units and syn- and postkinematic granites from Nanga Parbat using (1) U-Pb and Th-Pb ion microprobe data, (2) $^{40}Ar/^{39}Ar$ analysis on more than 100 biotite mineral separates, and (3) field and mineralogical observations. Our extensive sampling has provided a very large regional distribution of ages that can be used to delineate the extent and location of young and active structures and determine the areal pattern of cooling, thus supplying a powerful test of structural and exhumational models. Combined with recent structural observations (Edwards 1998; Schneider et al. 1999*a*; Butler et al. 2000; Edwards et al. 2000), data presented here suggest that the evolution of Nanga Parbat is punctuated by at least three thermal events since initiation of the India-Asia collision: initial collision-related metamorphism, Late Miocene doming, and Plio-Pleistocene pop-up and anatexis, overprinting the previous two episodes.

Geologic Framework

The NPHM is a structural half window of Indian-cratonic basement, bordered to the north by the Karakorum terrane and to the west and east by Cretaceous island arc rocks of the Kohistan-Ladakh terrane. The island arc overthrusted the Indian rocks from the north at 60–50 Ma (e.g., Smith et al. 1994) along the Main Mantle Thrust (MMT) (fig. 1). Nanga Parbat is a recent feature, having developed from a crustal-scale pop-up structure mechanism (Schneider et al. 1999*a*) resulting in a large pair of north-south-oriented antiforms (e.g., Madin et al. 1989; Treloar et al. 1991). The interior region of Nanga Parbat is composed of mostly monotonous, highly foliated tonalitic biotite gneisses flanked by more heterogeneous, calcareous, and pelitic metasediments along the margins (fig. 1). Most granites and gneisses yield U-Pb accessory mineral ages containing consistent Early Proterozoic inheritance (~1850 Ma) (Zeitler et al. 1989; Schneider et al. 1999*b*, 1999*c*) with a few (Cambro-Ordovician) exceptions (Zeitler et al. 1989; Foster et al. 1999*a*; this study). The signature of the initial Himalayan high-grade metamorphism, once thought to be absent or elusive (i.e., overprinted), has recently been detected. Recent discovery of an ~19-Ma granite, the Southern Chichi pluton (fig. 1), immediately adjacent to a massif-bounding shear zone (Schneider et al. 1999*b*), and Eocene monazite U-Pb and garnet–whole-rock Sm-Nd ages from the Indian cover metasediments (Foster et al. 1999*b*, 2000) documents the occurrence of Himalayan metamorphism and anatexis in the western syntaxis.

The central regions of the NPHM have experienced a notable petrological overprint in the past few million years involving coeval granulite-facies metamorphism, migmatization, granite intrusion, and pervasive fluid flow (e.g., Craw et al. 1994; Winslow et al. 1994; Butler et al. 1997; Poage et al. 2000). In central NPHM, migmatites with monazite U-Pb ages of 3.3 Ma and of known *PT* conditions suggest rapid cooling rates (>200°C/m.yr.) and >15 km of unroofing in the past 3 m.yr. (Zeitler et al. 1993). Concentric isograds that encircle the summit region culminate in cordierite-K-feldspar-sillimanite grade (fig. 1; Winslow et al. 1994; Poage et al. 2000). Petrologic and isotopic evidence (e.g., Chamberlain et al. 1995) suggests crustal-scale fluid flow resulting in penetration of meteoric water to depths, achieving temperatures of 600°C (Craw et al. 1994). Many hot springs occur within the Nanga Parbat massif, typically exploiting faults and shear zones as conduits (Chamberlain et al. 1995; George and Bartlett 1996; Reddy et al. 1997).

Exposed within the once structurally deepest and now youngest portions of the massif are a moderate number of undeformed, laterally extensive granitoid dikes and pegmatites, as well as a few small bodies of structurally concordant and discordant leucogranites. These rocks have crystallization ages of 3–1 Ma (Zeitler et al. 1993; Schneider et al. 1999*c*) in the summit region, such as Tato and Mazeno Pass, where most of the granites reside within the cordierite metamorphic zone. Granite ages within the massif increase to the north; dikes along the Indus and Astor River sections are 7–5 Ma (Zeitler and Chamberlain 1991) and as old as 10 Ma in the north, for example, Jutial (Schneider et al. 1999*c*). Generation of the larger leucogranites most likely began when Proterozoic migmatites and gneisses underwent partial melting through fluid-absent muscovite breakdown at temperatures of ~700°C and at pressures ~7 kbars (Butler et al. 1997). Furthermore, due to the similarity of granite ages to the ages of metamorphism and cooling in the summit regions, granite emplacement was apparently coeval with exhumation, leading to the

suggestion that some of the smaller Nanga Parbat melt products owe their origin to decompression melting (e.g., Zeitler and Chamberlain 1991).

Bounded by young faults (fig. 1), the overall structure of NPHM is that of a pop-up structure, having a dominant northwest-, subordinate southeast-vergence (Edwards 1998; Schneider et al. 1999*a*). Active faulting is common along the western margin and includes the Raikhot-Diamir thrust system, which places Indian basement over Quaternary glacio-fluvial gravels along the Indus River, cutting out the trace of the MMT (e.g., Madin et al. 1989). Southwest and along strike of the main Raikhot fault, the surface trace of the fault system changes its trend to become north-south and is termed the "Diamir shear zone" (Schneider et al. 1999*a*; Edwards et al. 2000). The Diamir shear zone is a ductile to brittle west-verging shear zone with a reverse sense of shear. Intricately involved within the shear zone is the Jalhari granite. Throughout the zone, leucogranite lenses, tens to hundreds of meters thick, that show little to no subsolidus deformation are separated by, or frequently grade into, layers of gneiss, tens to hundreds of meters thick, where deformation of the Jalhari granite has been localized (Edwards 1998; Edwards et al. 2000). These high-strain layers anastamose around the relatively undeformed granite lenses, which mark reverse faults that dip to the east. The deformed granite frequently takes on an augen gneiss appearance, showing significant subsolidus strain, including S-C relationships and porphyroclast asymmetry, both of whose sense of shear indicates east-side (Nanga Parbat summit) up.

The conjugate structure to the Raikhot-Diamir thrust system, in the framework of the overall pop-up mechanism, is the west-northwest dipping Rupal shear zone (Schneider et al. 1999*a*). The Rupal shear is a several-kilometer-wide belt of monotonous, noncoaxially sheared granitic orthogneiss with ubiquitous S-C fabric and augen asymmetry recording dextral and northwest-side (Nanga Parbat summit) up displacement (Edwards 1998; Schneider et al. 1999*a*). No significant tectonic accommodation of exhumation (e.g., detachment structure) has been documented within or near the Nanga Parbat massif (Schneider et al. 1999*a*), only local, normal-motion structures that allowed relatively minor exhumation (Edwards 1998). Detailed descriptions of the conjugate shear systems are presented and discussed in Edwards (1998) and Edwards et al. (2000).

Magmatic and Metamorphic Events: Sampling Strategy and Results

To constrain the timing of deformation and fabric development, we determined the U-Th-Pb crystallization ages of syn- and postdeformational granites from Nanga Parbat: five leucogranite dikes and four granitic/gneissic units (fig. 1). This is in addition to our other recently reported geochronologic results (Schneider et al. 1999*b*, 1999*c*). In only two cases were we able to separate and analyze zircons and monazites from the same rock. Analyzing both accessory minerals helped identify problems associated with interpretation of ion microprobe geochronology of reworked, high-grade rocks, namely matrix effects and Pb loss. However, previous experience with the ion microprobe where we analyzed both zircon and monazite from the same sample (Schneider et al. 1999*c*) indicated an agreement of these mineral ages for rocks as young as 1.4 Ma.

Analytical methods are presented in appendix 1, and detailed results from $^{208}Pb/^{232}Th$ monazite and U-Pb zircon analyses are listed in tables 1 and 2, respectively (the appendix, figure 7*b*, and tables 2–4 are available from *The Journal of Geology* free of charge upon request). U-Pb concordia are shown in figure 2, and Th-Pb monazite ages for the Jalhari granite are shown in a histogram (fig. 3).

Feldspar Lath Gneiss. A sample was taken from an outcrop of the "lath unit" (location *E* on fig. 1; sample gotodas in table 1, and fully described in Edwards 1998 and Edwards et al. 2000) at the Biji-Barai river confluence. This gneiss contains 1- to >4-cm laths of feldspar in a kyanite-garnet-mica quartzofeldspathic matrix. The laths are characteristic of this discrete unit, generally mapped along the margins of the massif near the basement-cover contact (Edwards 1998; Foster et al. 1999*a*). The unit in many places displayed signs of high strain (the feldspar laths characteristically forming augen structures) and mylonitic foliation, with strong grain-size reduction in the matrix. Zircons from the lath unit were small, white, and rounded grains and yielded Cambro-Ordovician $^{206}Pb/^{238}U$ ages at 500–450 Ma (fig. 2) with no detection of the typical Nanga Parbat Early Proterozoic inheritance or Pliocene overprinting.

MMT Dike. Sample IK-05 is a small, undeformed, tourmaline-bearing granitic dike that cross-cuts the high-strain fabric of the MMT. IK-05 is located along the Skardu Road in the Indus River gorge (5 km from Sassi; location *A* on fig. 1); although previous dikes had been dated along NPHM's western margin near Sassi (~5 Ma; Zeitler and Chamberlain 1991), no field relationships were described.

Table 1. Th-Pb Isotopic Data

Grain[a]	Age (Ma) $^{208}Pb/^{232}Th$	$^{208}Pb^*/^{232}Th$	$^{208}Pb^*$ (%)	Th (est. ppm)	Th/U
Rupal leucogranite dikes (Th-Pb monazite):					
RD2_g3sp1	1.06 (.06)	5.22×10^{-5} (3.18×10^{-6})	64.64	76,443	11.49
RD2_g4sp1	1.15 (.07)	5.67×10^{-5} (3.36×10^{-6})	70.77	98,752	8.31
RD2_g5sp1	1.09 (.07)	5.38×10^{-5} (3.40×10^{-6})	64.87	48,657	9.98
TAP_gMsp1	1.93 (.19)	9.56×10^{-5} (9.21×10^{-6})	74.12	145,684	15.02
TAP_gOsp1	1.82 (.11)	9.02×10^{-5} (5.48×10^{-6})	64.59	89,681	11.17
TAP_gKsp1	1.83 (.13)	9.06×10^{-5} (6.27×10^{-6})	65.62	100,276	14.25
TAP_gAsp1	1.78 (.12)	8.82×10^{-5} (5.94×10^{-6})	59.74	92,803	14.39
TAP_gCsp1	1.99 (.18)	9.86×10^{-5} (9.01×10^{-6})	67.31	123,926	14.7
TAP_gEsp1	2.32 (.20)	1.15×10^{-4} (1.01×10^{-5})	42.92	113,520	17.3
TAP_g1sp1	1.80 (.06)	8.88×10^{-5} (2.94×10^{-6})	76.23	48,266	14.61
TAP_g3sp1	1.73 (.06)	8.55×10^{-5} (3.02×10^{-6})	72.84	52,142	11.03
TAP_g4sp1	1.84 (.06)	9.11×10^{-5} (2.95×10^{-6})	74.83	61,771	15.34
TAP_g5sp1	1.91 (.10)	9.43×10^{-5} (5.04×10^{-6})	71.59	30,280	18.49
TAP_g6sp1	1.95 (.05)	9.63×10^{-5} (2.62×10^{-6})	81.32	44,208	17.37
TAP_g7sp1	1.80 (.07)	8.92×10^{-5} (3.27×10^{-6})	73.26	38,697	15.02
TAP_g9sp1	1.86 (.08)	9.21×10^{-5} (4.16×10^{-6})	58.59	47,539	12.61
TAP_g9sp1	1.80 (.06)	8.90×10^{-5} (2.84×10^{-6})	77.23	61,771	18.28
Jalipur augen gneiss (Th-Pb monazite):					
JAL_g4sp1	5.08 (.09)	2.52×10^{-4} (4.29×10^{-6})	93.52	31,323	8.48
JAL_g5sp1	5.15 (.05)	2.55×10^{-4} (2.55×10^{-6})	91.82	62,872	21.18
JAL_g7sp1	5.16 (.05)	2.55×10^{-4} (2.42×10^{-6})	93.53	73,538	16.13
JAL_g8sp1	5.21 (.06)	2.58×10^{-4} (3.03×10^{-6})	93.59	77,467	18.97
JAL_g9sp1@1	2.87 (.08)	1.42×10^{-4} (3.92×10^{-6})	84.06	26,047	6.02
JAL_g9sp2	2.18 (.11)	1.08×10^{-4} (5.27×10^{-6})	74.73	13,584	4.67
JAL_g8sp2	5.13 (.07)	2.54×10^{-4} (3.41×10^{-6})	93.10	55,911	15.16
JAL_g7sp2	5.11 (.05)	2.53×10^{-4} (2.59×10^{-6})	93.58	63,995	15.51
JAL_g6sp1	5.33 (.05)	2.64×10^{-4} (2.66×10^{-6})	92.96	118,446	18.69
Jalhari granite (Th-Pb monazite):					
DIAM_gSsp1	4.14 (.17)	2.05×10^{-4} (8.29×10^{-6})	88.54	207,174	2.85
DIAM_gHsp1	4.01 (.87)	1.99×10^{-4} (4.31×10^{-5})	87.40	308,395	8.56
DIAM_gDsp1	4.97 (.18)	2.46×10^{-4} (9.09×10^{-6})	85.83	145,683	3.93
DIAM_gBsp1	3.20 (.36)	1.59×10^{-4} (1.79×10^{-5})	79.45	142,845	1.61
DIAM_gKsp1	3.14 (.07)	1.55×10^{-4} (3.30×10^{-6})	81.12	109,735	2.01
DIAM_gYsp1	7.13 (1.08)	3.53×10^{-4} (5.37×10^{-5})	90.38	306,503	14.71
DIAM_gYsp2	5.41 (.77)	2.68×10^{-4} (3.83×10^{-5})	91.96	280,961	9.08
DIAM_g2s1	3.77 (.14)	1.86×10^{-4} (6.73×10^{-6})	74.81	85,731	1.88
DIAM_g2s2	3.55 (.13)	1.76×10^{-4} (6.64×10^{-6})	75.32	85,518	1.79
DIAM_g2s2@1	3.78 (.06)	1.87×10^{-4} (2.93×10^{-6})	85.57	84,774	1.79
DIAM_g11(k)s1	3.33 (.17)	1.65×10^{-4} (8.41×10^{-6})	73.03	82,434	1.97
DIAM_g25(y)s1	6.86 (.10)	3.40×10^{-4} (4.80×10^{-6})	89.07	248,897	13.23
DIAM_g25(y)s1@1	7.17 (.04)	3.55×10^{-4} (2.22×10^{-6})	91.87	246,770	13.65
DIAM_g25(y)s2	5.94 (.07)	2.94×10^{-4} (3.42×10^{-6})	87.91	231,878	11.16
DIAM_g26(z)s1	5.62 (.10)	2.78×10^{-4} (4.71×10^{-6})	86.26	180,823	7.75
DIAM_g23(w)s1	7.81 (.13)	3.87×10^{-4} (6.31×10^{-6})	89.12	255,279	23.16
DIAM_g19(s)s1	4.35 (.11)	2.15×10^{-4} (5.31×10^{-6})	81.68	130,830	3.41
DIAM_g16(p)s1	6.40 (.07)	3.17×10^{-4} (3.59×10^{-6})	88.72	258,470	11.77
DIAM_g15(p)s1	5.94 (.09)	2.94×10^{-4} (4.65×10^{-6})	87.29	221,242	9.30
DIAM_g13(m)s1	5.28 (.12)	2.61×10^{-4} (6.16×10^{-6})	85.70	207,414	8.74
DIAM_g8(h)s1	7.90 (.10)	3.91×10^{-4} (4.74×10^{-6})	91.28	353,136	26.51
DIAM_g8(h)s2	2.27 (.22)	1.12×10^{-4} (1.07×10^{-5})	65.72	187,205	6.88
DIAM_g8(h)s2@1	2.61 (.04)	1.29×10^{-4} (1.82×10^{-6})	84.55	182,950	7.17
DIAM_g4(d)s1	5.10 (.13)	2.52×10^{-4} (6.22×10^{-6})	81.46	108,494	4.72
DIAM_g22(x)s2	2.37 (.31)	1.17×10^{-4} (1.51×10^{-6})	58.03	119,130	3.08
DIAM_g21(u)s1	5.78 (.08)	2.86×10^{-4} (3.91×10^{-6})	86.94	216,987	8.12
DIAM_g21(u)s1@1	6.00 (.04)	2.97×10^{-4} (2.11×10^{-6})	92.14	219,114	8.18
garal_g3sp1	13.29 (.52)	6.58×10^{-4} (2.57×10^{-5})	96.08	78,590	28.94
garal_g3sp2	12.55 (.32)	6.21×10^{-4} (1.59×10^{-5})	95.39	58,942	26.88
garal_g3sp3	13.37 (.58)	6.62×10^{-4} (2.85×10^{-5})	96.54	70,731	30.00
garal_g3sp4	13.11 (.43)	6.49×10^{-4} (2.13×10^{-5})	96.07	63,995	29.31

Note. Standard errors in parentheses.

[a] g = grain; sp = spot; @1 = a subsequent analysis on an existing spot.

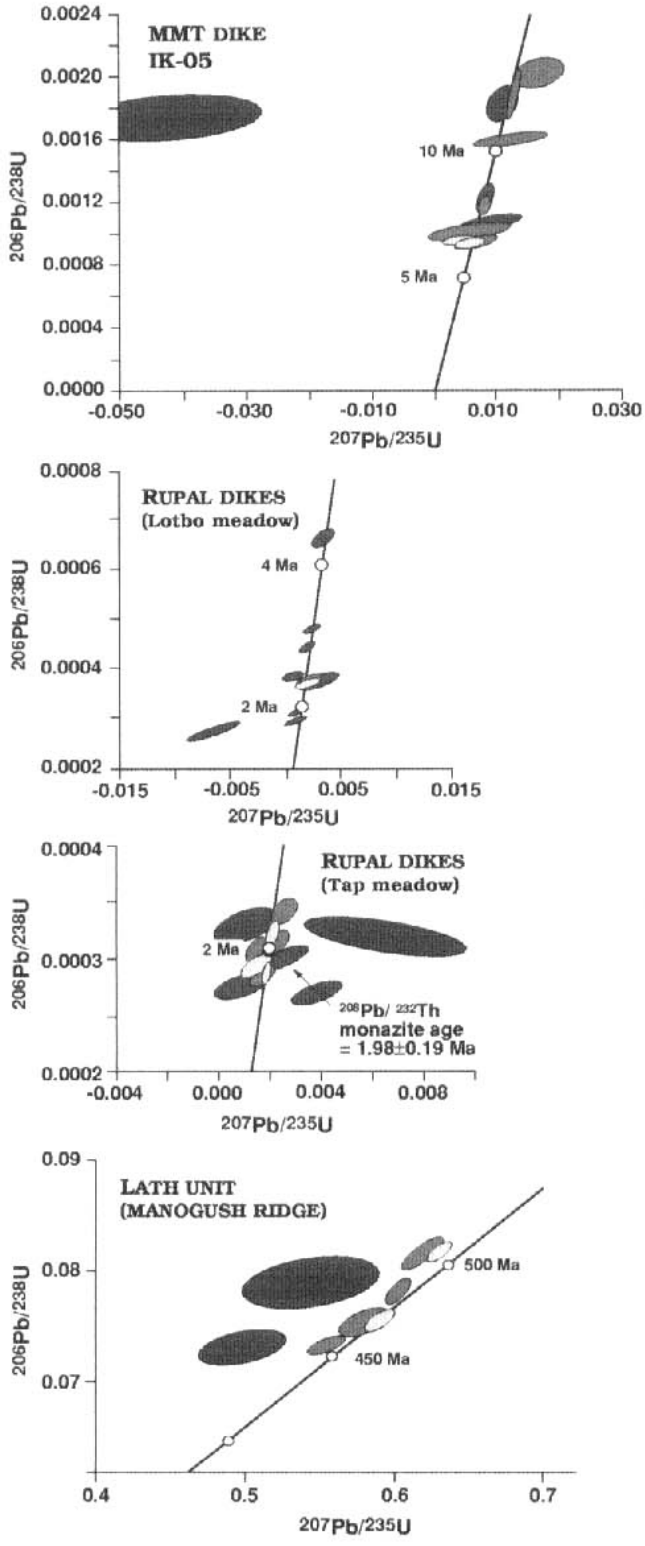

Figure 2. U-Pb concordia plots showing zircon spot ages of granitic rocks discussed in this study. Error ellipses are shown at 1σ level. Table 2 has complete isotopic data.

Sample IK-05 yielded distinctly blue euhedral zircons with two age populations: Early Proterozoic (~1850 Ma) and a scatter of apparently concordant ages from 13 to 6 Ma (fig. 2). The Early Proterozoic ages are ubiquitous throughout the granites and gneisses of Nanga Parbat (Zeitler et al. 1993; Schneider et al. 1999*b*, 1999*c*) and represent inheritance from an Indian craton protolith. The scatter in the younger concordant ages also suggests possible inheritance from a second source. There is evidence for a Middle to Late Miocene anatectic event <10 km north and west of the IK-05 sample locality. The Jutial pluton, a large 9.5 ± 0.1-Ma granite (Schneider et al. 1999*c*), is located directly north of the granite dike. In addition, the Rb/Sr and $^{40}Ar/^{39}Ar$ ages from gneisses and granites along the massif's margin and from granite sheets from within the adjacent Kohistan arc are 18–13 Ma (George et al. 1995). This Middle to Late Miocene melting episode is preserved in the zircon as a growth rim, overprinted by the latest (~7 Ma) melting. Alternatively, the younger concordant ages may be hydrothermal in origin and reflect the timing of fluid migration through the shear zone. Both

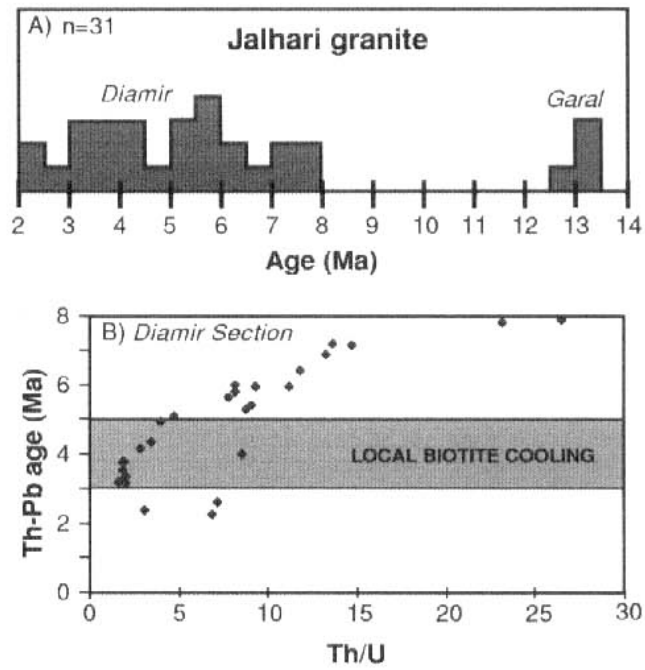

Figure 3. *A*, Histogram of Th-Pb ages obtained from ion microprobe spot analyses of monazites from the deformed (Diamir) and undeformed (Garal) section of the Jalhari granite. *B*, Plot of Th/U versus age for the Diamir section of the Jalhari granite. Younger ages are coincident with biotite cooling ages and other monazite ages along the western margin. See text for discussion.

cases are supported by the presence of faint zircon rims imaged with a scanning electron microscope (SEM). Accounting for the older Miocene concordant ages of IK-05 as a separate metamorphic episode resulted in a cluster of spot analyses with a weighted average zircon $^{206}Pb/^{238}U$ age of 6.94 ± 0.75 Ma, which we suggest as the final age of granite crystallization. Although previously reported scattered concordant Nanga Parbat ages appear to have been affected by xenotime and apatite inclusions within the zircon grains (Schneider et al. 1999*c*), we saw no strong evidence of this phenomenon here.

Rupal Leucogranite Sheets. Also sampled were four leucogranite dikes in central Rupal Valley, west of Bezhin glacier and immediately south of the Nanga Parbat summit (location *F* on fig. 1). In the apparently localized "dike swarm" in the northern valley wall (the Rupal face), we sampled three leucogranite dikes from the walls above Tap meadow and one dike from Lotbo meadow to the west. The predominantly undeformed, structurally discordant tourmaline-pegmatitic dikes are 1–2 m thick and are typically oriented north-northeast and dip moderately west. Crystallization ages on all of these post-fabric leucogranite sheets therefore provided a minimum age of local displacement on the Rupal shear zone.

Zircons from the Rupal dikes are distinctly blue euhedral grains; monazites are greenish-yellow anhedral grains. Analyses from the Rupal dikes yielded very young ages, but showed no evidence for Early Proterozoic inheritance (fig. 2). The most southern and western dike examined was a sample from Lotbo (LTB), which yielded concordant analyses ranging in ($^{206}Pb/^{238}U$) age from 4.3 to 1.8 Ma. The spread in these analyses was a little difficult to resolve and has been documented in other zircon analyses from very young rocks (e.g., Zeitler et al. 1993). It may be related to the high-U content of the zircons (cf. Parrish and Carr 1994) or inheritance of zircon crystallized during the 4–3-Ma metamorphism that is common in the summit regions (Smith et al. 1992). In any case, a number of spot ages from this granite dike were ~2.3 Ma, but the general scatter was too great to be explained by analytical imprecision and probably represented xenocrystic inheritance. Zircon analyses from a second Rupal dike (TAPz) tightly clustered at 2 Ma and did not give a spread of ages. A weighted average zircon $^{206}Pb/^{238}U$ age of 1.95 ± 0.14 Ma for this sample is supported by monazite analyses from the same granite dike (TAPm), which yielded an indistinguishable weighted average $^{208}Pb/^{232}Th$ monazite age of 1.98 ± 0.19 Ma (table 1). Monazites from the remaining two granite dikes yielded Th-Pb weighted average ages of 1.84 ± 0.07 Ma for sample TAP2 and 1.10 ± 0.04 Ma for sample RD2 (table 1). The latter sample was both the topographically highest (4200 m) and farthest north (by ~1 km) of all the Rupal dikes sampled in this study. As stated, none of the Rupal granite dikes yielded the Early Proterozoic inheritance seen throughout the massif, even in Rupal Valley itself (Schneider et al. 1997, 1999*c*); moreover, the concordancy between U-Pb zircon ages and Th-Pb monazite ages suggested that no U-disequilibrium exists in the U-Pb ages, which has been recorded elsewhere in young rocks (cf. Barth et al. 1989).

Patro Gah Augen Gneiss. A mafic-rich, porphyroclastic granitic gneiss (location *B* on fig. 1; sample JAL in table 2) located within the Raikhot fault system was sampled from the first bedrock ridge high above the Jalipur sandstones, along the Karakorum Highway at the entrance to Patro Gah. Coarse asymmetric feldspar grains showed predominantly top to the northwest thrust sense, consistent with observations farther along the fault at Tato and Lichar. The Patro augen gneiss yielded fairly euhedral and transparent green monazite and a weighted average Th-Pb age of 5.16 ± 0.08 Ma for all but two spot analyses (JAL_gr8sp2 and JAL_gr9sp1@1; table 1). These two analyses contained somewhat lower $^{208}Pb^*$, which suggests hydrothermal replacement.

Jalhari Granite. From the southwestern margin of the massif, two samples of the Jalhari granite (Edwards et al. 2000) came from within the Diamir shear zone (locations *C* and *D* on fig. 1). The first (sample DIAM in table 1) was a deformed, altered-biotite-rich portion of the granite collected near the village of Diamroi. The granite sample contained sheared garnets and was severely retrograded. Petrographic assessments of prevailing deformation mechanisms suggested deformation of the Jalhari granite probably occurred at >500°C, indicated by sutured feldspar grain boundaries and neocrystallized grains on margins of larger grains (Edwards et al. 2000). Field measurements showed foliation in deformed portions of the granite is moderately to steeply east-southeast-dipping. Near the village of Garal, 13 km south of Diamroi and along strike of the shear zone, we sampled an undeformed medium-grained granite (sample garal in table 1), interpreted to be part of the same ~5-km-wide, ~30-km-long plutonic sequence that defines the Jalhari granitic units (Edwards et al. 2000).

Zircons from a deformed portion of the Jalhari granite are white, rounded grains; monazites are fairly euhedral and transparent green grains. Zircons

analyses yielded the typical Nanga Parbat Early Proterozoic signature with spot analyses falling along a discord (table 2), with an unresolvable lower intercept, suggesting the granite is a melt product of the adjacent reworked Nanga Parbat gneisses. Jalhari granite monazites, however, yielded possibly surprising results. Of the 15 or so original monazite grains selected from the undeformed Jalhari granite (at Garal), only a limited number of monazite analyses were obtained, due to problems with sample mount preparation; these four analyses yielded ~13-Ma ages (table 1). Monazite spot analyses from the deformed section of the Jalhari granite in Diamroi Gah gave much younger dates than the undeformed Jalhari granite monazite age. From a single granite sample, we obtained a range of Th-Pb ages from 8 to 2 Ma (fig. 3) with errors typically ± 0.20 Ma but as high as 1 Ma in one case (table 1). The weighted average Th-Pb age of the deformed section of the Jalhari monazites is 4.89 ± 1.66 Ma, which is probably geologically meaningless.

It is of interest that the Th-Pb dates have a positive correlation with the Th/U of each spot analysis (fig. 3), which was obtained during ion microprobe analyses. This indicates that the relatively higher-U spot analyses yielded younger ages, opposite from the results that Harrison et al. (1999) obtained from the Manaslu complex. Harrison et al. (1999) showed that monazite ages from the younger of two intrusive phases of the complex (Bimtang) have high Th/U, and the older phase (Larkya La) ages have lower Th/U. Our analyses were conducted over two separate probe sessions, repolishing the probe mount between sessions, and a calibration curve was established using two different reliable monazite standards (554 and 4170; appendix 1). Care was taken to control surface charging and crater depth of the sample during analysis, which can affect the density distributions of Th^+ and Pb^+ during sputtering. Further, an aperture was inserted into the beam path to reject secondary ions emitted from near the edge of the crater, where the extraction field is far from uniform. We feel confident that the Jalhari monazite dates are not an experimental artifact but can be explained geologically (see "Discussion").

Bedrock Cooling and Exhumation: Sampling Strategy and Results

To reveal the cooling age pattern across Nanga Parbat, more than 150 samples were collected from the massif (figs. 4, 5), concentrating on the region south of the Indus-Astor River confluence. Transects were made along the major valleys of the massif (Thak, Niat, Bunar-Biji, Diamir, Airl, Rupal, Chichi, and Rama), along the two major river valleys crosscutting the massif (Indus and Astor), and over Mazeno Pass, which connects the southern and western valleys. Samples were also taken from the Haramosh region and the mafic island arc rocks of the Kohistan terrane. Sampling was restricted by relief, abundant talus slopes along the valley walls, and the military exclusion zone next to the political boundary in the south and southeast (Pak-Indo cease-fire line). This approach complemented previous thermochronologic studies undertaken along the western margin (e.g., George et al. 1995) and in Tato (e.g., Winslow et al. 1996). The mineral of interest for our cooling study was biotite because it is extremely abundant (40% of total rock in some cases) in both the Nanga Parbat gneisses and the adjacent Indian cover metasedimentary sequences and because it represents a good intermediate closure temperature mineral that can be rapidly analyzed. The closure temperature for biotite during rapid cooling is ~340°C (Baldwin et al. 1993) and is a good proxy for the estimated temperature of the brittle-ductile transition zone in quartzofeldspathic rocks. By dating biotite, we can constrain the timing of strain-related fabric and also assess the cooling and exhumation history of the region.

Analytical methods are presented in appendix 1, and detailed results from $^{40}Ar/^{39}Ar$ analyses are located in tables 3 and 4 and figure 7*b*. Results were plotted as sample locations in figures 4 and 5 and contoured in figure 6. Figure 7*a* shows $^{40}Ar/^{39}Ar$ incremental age spectra, and figure 7*b* shows respective $^{39}Ar/^{40}Ar$ versus $^{36}Ar/^{40}Ar$ isotope correlation diagrams. Correlation diagrams (fig. 7*b*) were used to quantify the amount of excess Ar incorporated into the biotites, which was assumed to be, and was plotted as, an $^{40}Ar/^{36}Ar$ intercept of 295.5, the present-day atmospheric value. Previous detailed $^{40}Ar/^{39}Ar$ investigations at Nanga Parbat indicated that most metamorphic silicate minerals contain excess Ar ($^{40}Ar/^{36}Ar = 400$) and produce erroneously old cooling ages (Reddy et al. 1997; Whittington 1997). None of our results indicated an excess component of more than $^{40}Ar/^{36}Ar = 373$ except possibly in two cases where the $^{40}Ar/^{36}Ar$ intercept may be >2000; in these cases, our results should be viewed as cooling age maximas. Sensitivity tests showed that even if the $^{40}Ar/^{36}Ar$ intercept was as high as 400, the excess component of Nanga Parbat rocks reported in Reddy et al. (1997), our ages would decrease by only 0.4–0.5 Ma. We are confident that our total-fusion ages and step-heated ages are good approximations for the time of cooling through ~350°C for the core rocks at

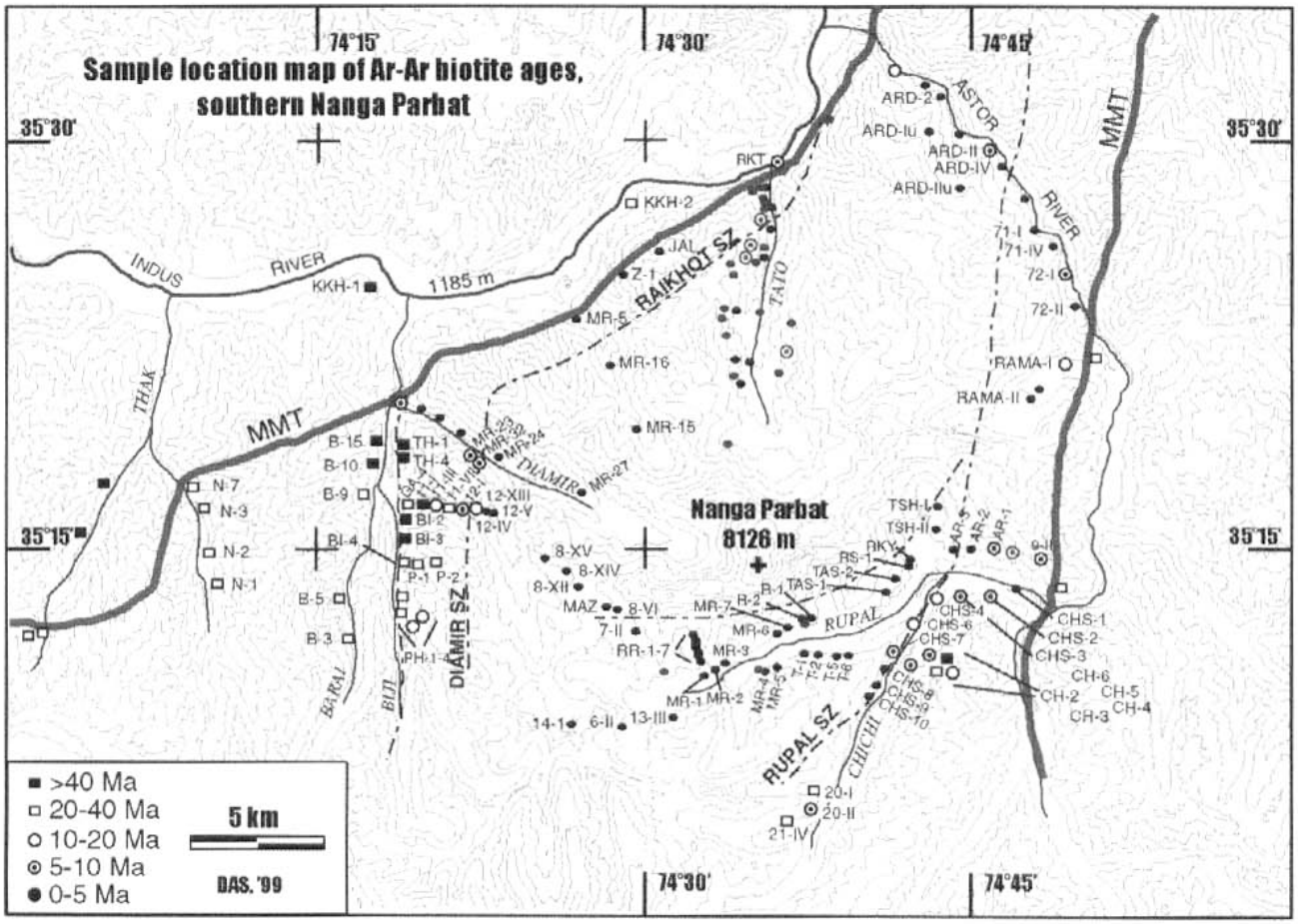

Figure 4. Sample location map of Ar-Ar biotite ages from rocks south of the Indus-Astor River confluence, Nanga Parbat area. Locations are plotted as age-related symbols. Boundaries of the two major thrust fault systems (Schneider et al. 1999*a*) are demarcated by dashed lines. Symbols not labeled (e.g., Tato) are results from previous studies (Zeitler and Chamberlain 1991; Winslow et al. 1996; Whittington 1997). Tables 3 and 4 have complete isotopic data.

Nanga Parbat. Further, young total-fusion dates with low radiogenic yields may be inaccurate by as much as 25%–50%, but the large number of concordant analyses over such a geographic region should attest to the robustness of the first-order thermochronologic picture.

To facilitate interpretation with respect to the main geologic structures, we divided our biotite $^{40}Ar/^{39}Ar$ cooling ages into three categories: cover, core, and shear zone (tables 3, 4). Cover rocks were sampled from the Indian metasedimentary sequence (pelites, marbles, gneisses, amphibolites) along the margins of the massif. Also included in this group were samples taken from the surrounding (Kohistan-Ladakh) island arc terrane. Shear zone rocks are samples taken from either of the two main conjugate thrust structures, the Raikhot-Diamir shear zone or the Rupal-Chichi shear zone. The northern margin of the Rupal shear is apparently not a discrete feature; the shear zone margins have migrated over time (Edwards 1998; Schneider et al. 1999*b*). Nonetheless, our samples collected throughout the Rupal Valley are representative of the shear zone section. Core rocks represent the samples of Nanga Parbat biotite gneisses bounded by the shear zones and were taken, generally, from the inward reaches of the valleys.

Cover Rocks. Laser total-fusion biotite cooling ages from the Indian cover sequence at Nanga Parbat vary in age from ~5 to >100 Ma. Typically, however, cooling ages are 30–20 Ma for rocks from the southwest (fig. 4; table 3); a few ages are significantly older near the contact with the Diamir shear zone, undoubtedly due to shear zone fluid-related excess Ar. Our Oligocene to Early Miocene cooling ages are similar to the cooling ages in the Babusar Pass area (Chamberlain et al. 1991) and in adjacent Kohistan (Treloar et al. 1989), and similar to the

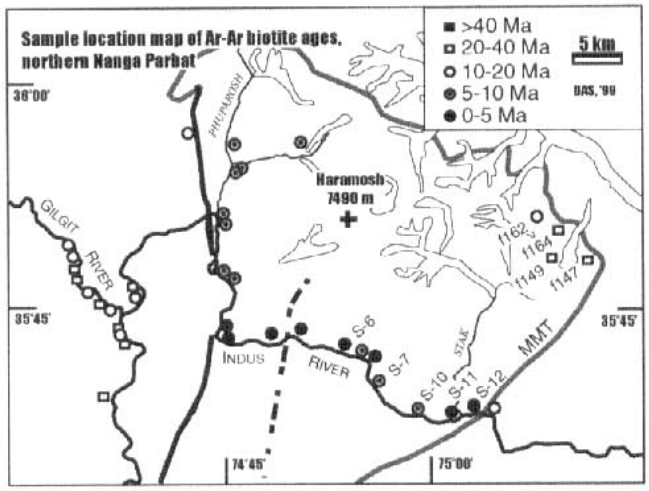

Figure 5. Sample location map of Ar-Ar biotite ages from rocks north of the Indus River, Haramosh area. Locations are plotted as age-related symbols. Geologic boundaries after Schneider et al. (1999*a*). Symbols not labeled are results from previous studies (Treloar et al. 1989; George et al. 1995). Tables 3 and 4 have complete isotopic data.

cooling ages farther southwest in the Indian plate rocks of the Hazara syntaxis (Treloar and Rex 1990). Further cooling revealed by ~16–15-Ma zircon fission-track ages from west of Nanga Parbat in the upper Kaghan Valley and in Kohistan (Zeitler 1985) is consistent with our $^{40}Ar/^{36}Ar$ data. In the cover rocks of the southeast portion of the massif, cooling ages are at 20–10 Ma, with a few slightly younger ages near the contacts of the Rupal shear zone and in the core rocks. Cover rocks in the far northeast corner are also relatively old, >10 Ma. The few younger ages within the cover sequence along the eastern margin may represent biotite-chlorite retrogression associated with the brittle Churit fault (Edwards 1998).

Step-heated samples also indicated older cooling in the cover sequence (fig. 7*a*). Sample S-10 is slightly younger than the remaining cover samples, but its location is near the core-cover boundary that may have impacted the cooling age during uplift. Several of the samples are highly radiogenic, represented by a cluster of points at the $^{39}Ar/^{40}Ar$ axis on the correlation diagrams, making it difficult to assess the excess Ar component. In two cases (f164 and f149), the correlation diagrams suggested an almost horizontal array of points, indicating an $^{40}Ar/^{36}Ar$ intercept of 1000–2000, and thus in these two cases there may be significant excess Ar. This only affects the ages by 4–8 m.yr., however, and the ages remain older than the core rocks. The step-heated ages from southern Nanga Parbat do not show this level of excess Ar and probably record cooling during the Oligocene. The majority of the cover sequence at Nanga Parbat apparently had a simple cooling history since the initial "post-Himalayan" metamorphic cooling and has since not been thermally disturbed.

Core Rocks. Eighteen samples of the Nanga Parbat biotite gneiss within the core were processed for laser total-fusion $^{40}Ar/^{39}Ar$ analyses. These ages are <5 Ma (except in one case in the north) and as young as ~1 Ma for samples closer to the summit (fig. 4; table 3). This is consistent with biotite cooling ages from other studies of the massif (e.g., Winslow et al. 1996; Whittington 1997; Treloar et al. 2000) and with the fission-track ages of Zeitler (1985) with cooling ages that become older to the northwest (e.g., George et al. 1995). Some of the data suggested an apparent age gradient with elevation (e.g., higher samples like MR-15 and 8-XIV have younger ages), but because of probable excess Ar in some samples (e.g., 8-XII), exact values are unresolvable.

Step-heated samples (fig. 7*a*) further confirmed young ages in the core rocks. These four spectra typically have an old first increment, which plots as atmospheric Ar (295.5) on the correlation diagrams, and a relatively old last increment. The remaining increments on the age correlation diagrams yielded a relatively linear array with MSWDs of <3 for three samples and negligible excess Ar. The core rocks represent the hanging wall of both of the major conjugate-thrust shear zones and the young ages indicate recent unroofing.

Shear Zone Rocks. Total-fusion biotite cooling ages from the Diamir shear zone ranged from <2 Ma to generally 15–10 Ma, with two samples yielding ages >30 Ma (fig. 4; table 3). The two young samples (Z-1 and Jal) yielding ages <2 Ma were located in the central section of the shear zone between the Tato and Diamir Valleys (fig. 4). These ages are more consistent with shear zone cooling ages in northern Tato (e.g., Winslow et al. 1996) and with the ages we obtained for the adjacent core gneisses than with the older cooling ages (average ~12.5 Ma) in the southern portion of the shear zone system (Diamir, Airl, Biji Valleys). Thus the older Diamir shear zone samples have cooling ages older than the core gneisses but not as old as the nearby cover sequence.

Two step-heated samples from the Diamir-Raikhot shear zone supported the total-fusion results. Sample MR-5 yielded a similar age to those of the core rocks with an initial old increment and a relatively linear array on the correlation diagram

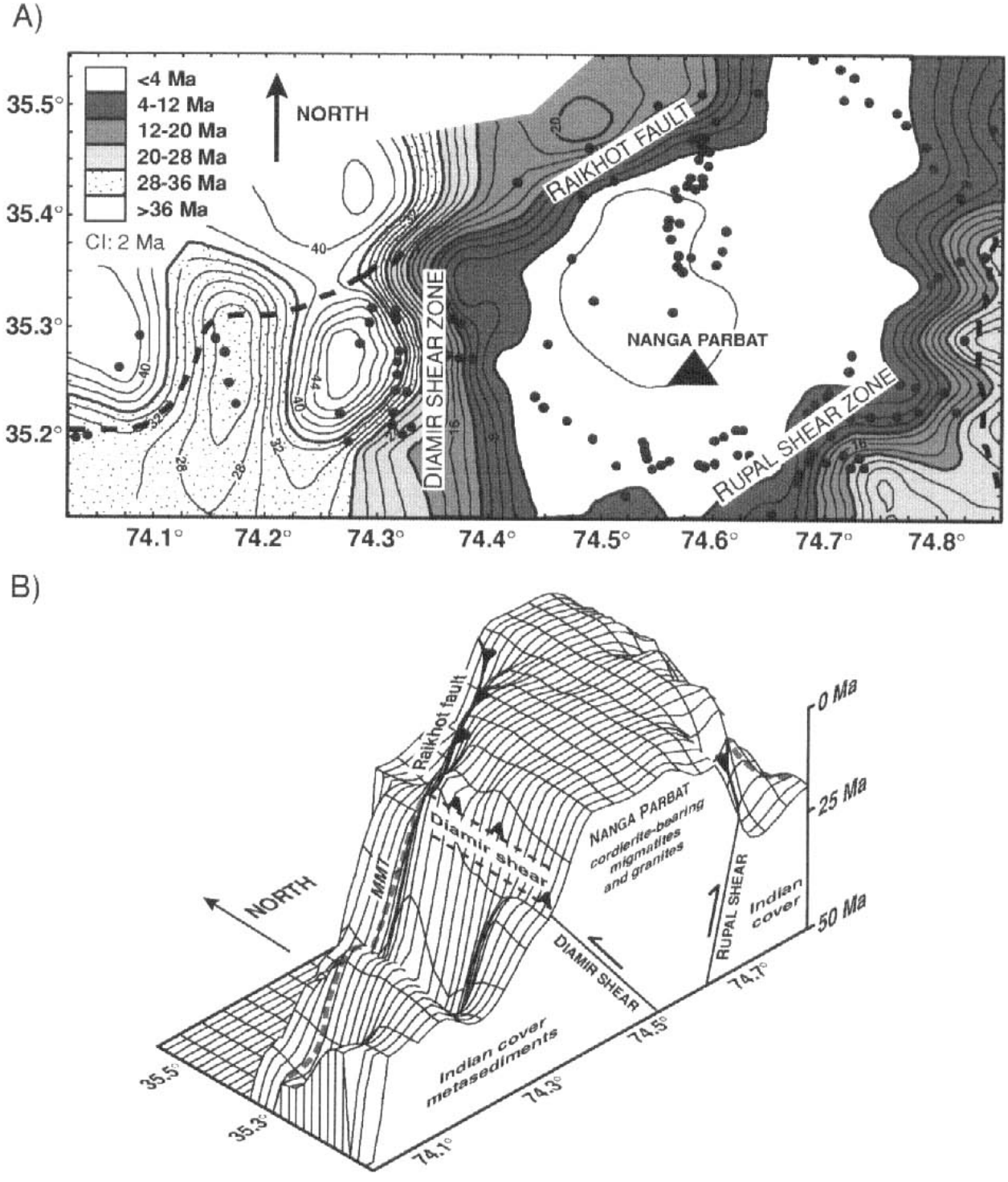

Figure 6. *A*, Contoured Ar-Ar biotite cooling map of Nanga Parbat. *B*, Perspective view of same map (Schneider et al. 1999*a*). Note the marked age gradient on all sides of the summit region. Main structures are noted and dashed line is the approximate location of MMT. For structures shown, no implication of the age axis corresponding with depth is intended.

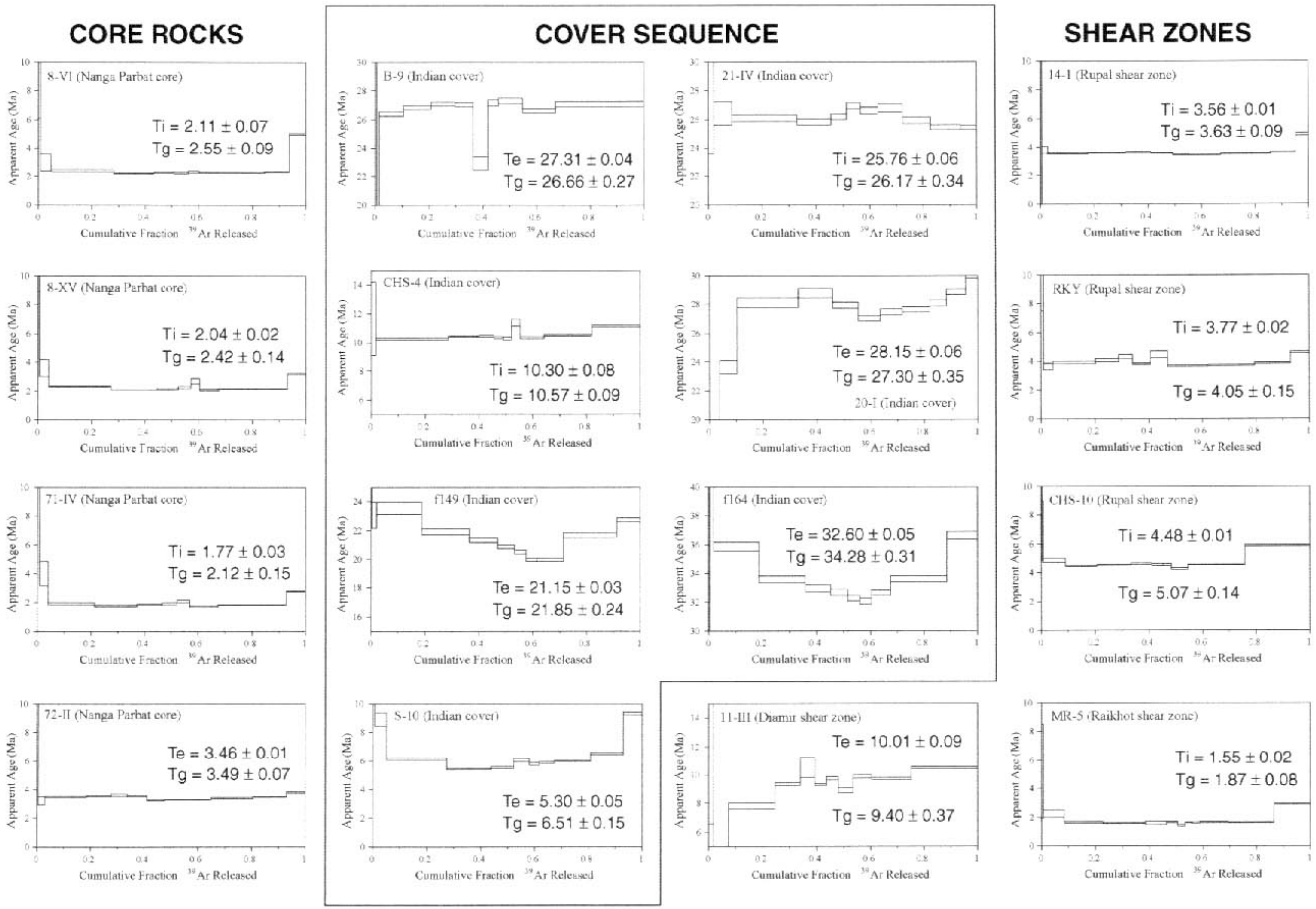

Figure 7*a*. Ar-Ar incremental step-heating age spectra. Errors are at 2σ level. All spectra are plotted in a 10 m.yr. window. *Tg*, total gas age; *Ti*, isochron age (MSWD < 3); *Te*, errorchron age (MSWD > 3); 40/36 and ages were calculated using a York fit regression.

resulting in an isochron age of 1.55 ± 0.02 Ma. This sample was also near Z-1 and Jal, which yielded <2-Ma total-fusion ages. Sample 11-III additionally confirmed the Late Miocene total-fusion ages of the Jalhari granite with an errorchron age of 10.01 ± 0.09 Ma. Isotope correlation did not show an excess Ar component.

The Rupal shear zone yielded younger total-fusion biotite cooling ages than the Diamir section of the Diamir-Raikhot shear zone. Ages from the Rupal area are from <5 to <2 Ma, similar to the core gneisses on the north side of the summit; there is no apparent significant age pattern within the Rupal shear or within the Rupal Valley. Along the southeastern margin of the Rupal shear, as well as in the upper Rupal Valley, the ages are the oldest (~5 Ma), and the cooling ages become older farther east toward the cover rocks. Results were consistent with those of Whittington (1997), who obtained older cooling ages in Rupal near the eastern cover contact.

Step-heated isochron ages (fig. 7*b*) also indicate cooling within the Rupal shear zone at <5 Ma. On the basis of our correlation diagrams, the excess Ar component is probably minimal and, like the core rocks, is probably not more than $^{40}Ar/^{36}Ar \leq 400$.

Cooling Summary. In general, the first-order appearance of the cooling age pattern of Nanga Parbat represents cooling associated with the pop-up mechanism that caused it (fig. 6). Recent exhumation appears to be restricted to inboard of the pop-up structure and thus to the higher topography within the massif. We have shown that the biotite cooling ages are only minimally affected by excess Ar ($^{40}Ar/^{36}Ar \leq 400$), supporting Reddy et al.'s (1997) conclusions. However, it is noted that all data from this region need careful interpretation regarding excess Ar, fluid interaction, and proximity to shear zones, and that differences in the apparent age of samples are not necessarily real. When differences between nearby samples are often ±1 m.yr., it seems unwise to attribute similar apparent age differences between samples to differential erosion across structures that are largely hidden by glaciers and moraines, and hence largely unmapped. Through large numbers of analyses, as presented in this study, and by careful interpretation of isotope correlation diagrams, it has been shown that large differences in apparent ages do indeed show marked age gradients across the mapped major structures into the much older cover sequence.

Discussion

Basement Rocks. The majority of the exposed granites and gneisses of the core and cover sequences at Nanga Parbat yield Early Proterozoic (~1850 Ma) inheritance ages in zircons and monazites alike (Zeitler et al. 1989; Smith et al. 1992; Schneider et al. 1999*b*, 1999*c*; this study). Early Proterozoic protolith ages are consistent with Nd model ages of the basement units (Whittington et al. 1999) and suggest a deeper level of erosion through the Greater Himalayan Sequence, exposing the Lesser Himalayan Sequence. Our new results on the feldspar lath unit at Manogush indicated that it is a discrete unit of Cambro-Ordovician age, markedly younger than the other basement units in the massif. A petrologically similar strained gneiss was described by Edwards (1998) on the southeast side of Nanga Parbat (Astor Valley). Foster et al. (1999*a*) obtained ~500-Ma SHRIMP monazite ages from the cores of garnets within this lath unit. Zeitler et al. (1989) reported zircons from a sample of the Shengus gneiss in northwest Nanga Parbat, yielding a 500-Ma inheritance; monazite U-Pb ages from the Shengus, however, yield Early Proterozoic ages (Smith et al. 1992), implying the entire Shengus unit probably does not have the same protolith. These three separate outcrops, however, reside in or near the generally agreed-upon lithological and structural contact between the Nanga Parbat gneisses and the cover sequence. Cooling ages of the Cambro-Ordovician units, reported here, are not dissimilar to cooling ages of the surrounding basement gneisses. On the basis of (1) the basement-cover relationship across a large area, (2) the age, and (3) the similar petrologic nature of the west and east localities, we suggest that the Cambro-Ordovician lath unit is a deformed product of an originally, largely continuous, granitoid unit within the massif, intruding into or near the current "basement-cover" contact. Edwards et al. (2000) have suggested that the unit provided a mechanical instability, which allowed portions of the original intrusive bodies to become highly strained during hypothesized MMT footwall ramp duplex development that is associated with the main displacement of the MMT. The unit may be faulted and eroded away along much of the active western margin of the massif. Other areas in the Himalaya (Pakistan, India, Nepal) also contain evidence for Cambro-Ordovician intrusions, and these are documented to have affected a substantial portion of the northern margin of the Indian craton (e.g., Le Fort et al. 1986).

Granite Dikes. The crystallization ages of the granites in this study provided significant constraints on the timing of deformation along the margins of the Nanga Parbat massif. Ages on the smaller, undeformed leucogranite dikes and the na-

ture of their crosscutting relationships provided us with minimum age estimates of displacement on shear zones. Sample IK-05 gave a crystallization age of ~7 Ma, consistent with other smaller leucogranite dikes along the western margin of the massif, which gave accessory mineral ages between 7 and 5 Ma (Zeitler and Chamberlain 1991; Schneider et al. 1999*c*). IK-05's cross-cutting association with the local high-strain rocks of the MMT requires that local deformation along the MMT ceased by at least 7 Ma. A number of geochronologic studies have determined that the youngest movement on the MMT along the NPHM northwestern margin (north of Astor River gorge) is between 12 and 8 Ma (George et al. 1995; George and Bartlett 1996; Reddy et al. 1997; Whittington 1997). Bedrock cooling ages (e.g., George et al. 1995; this study) along the Indus River Valley through the massif are generally 10–5 Ma and further suggest relatively cool, tectonically quiet rocks since that time. This supports the conclusions of Pêcher and Le Fort (1999), who suggested that ductile deformation on the northern Nanga Parbat-Karakorum contact zone ended around 7–6 Ma, on the basis of structural and geochronologic data in and around the suture zone. Continuity of structures and cooling ages across the main sutures suggest the entire region behaved as a single coherent crustal block through Late Miocene deformation and cooling, producing only localized domes. This Miocene deformation in the north (Haramosh and adjacent Karakorum) was a result of collisional transpression (see below) (Pêcher and Le Fort 1999).

The Rupal dikes, similar to the MMT dike, provide key timing constraints on structures and fabrics of the Rupal Valley; the oldest crystallization age gives the minimum age of displacement. In this case, the structurally lowest sample, LTB, was the oldest dike dated in this study and gave an age of 2.3 ± 0.4 Ma. Thus ductile displacement on this segment of the Rupal shear zone ceased (stepped?) before ~2.5 Ma. Granite dikes toward the summit yielded consistently younger ages with the highest and farthest summitward yielding a crystallization age slightly older than 1 Ma (sample RD2). Furthermore, dike emplacement was coeval with cooling: the dike ages are similar to the $^{40}Ar/^{39}Ar$ biotite cooling ages in the Rupal Valley (e.g., Stanfill 1997). This suggests the dikes were emplaced into shallow crustal levels where country rock temperatures were ~350°C, the melt having possibly migrated along portions of the Rupal shear and into fractures accompanying uplift and unroofing. Biotite cooling data suggest that the larger granites at Mazeno Pass and Tato also intruded into relatively cool (~350°C) basement rocks, probably near the zone of brittle-ductile transition (6–7 km), leading Schneider et al. (1999*c*) to suggest granite emplacement was arrested by general strength contrasts across the transition zone. Granite emplacement into cool rocks at Nanga Parbat was also documented in the Rupal and Tato Valleys by Whittington (1997).

The Rupal dikes are also similar to dikes and melt stringers on the north side of the summit in age and structural orientation. Crystallization ages of granites in Tato are at 3–1 Ma (Zeitler et al. 1993) and were emplaced, and somewhat deformed, in the southeast-dipping Raikhot shear zone, the conjugate of the north-northwest-dipping Rupal shear. In contrast, crystallization ages south of Rupal are significantly older. Monazite crystallization ages of a thin leucogranite dike, which cross-cuts the fabric of the southeastern margin of the Rupal shear in Chichi Valley, combined with the biotite cooling ages of adjacent shear zone and cover rocks that we present here, require that displacement of this portion of the shear zone predates ~10 Ma (Schneider et al. 1999*b*). Overall, the age pattern recorded in biotite cooling and granite crystallization ages suggest that recent tectonic activity is restricted to the core rocks or summit regions of Nanga Parbat (fig. 6). This activity not only represents recent melting and cooling but also minimum age estimates on cessation of ductile deformation, consistent with our previous suggestion that deformation has migrated inward within the massif (Schneider et al. 1997, 1999*c*).

Granitoids. The spread of monazite ages in the deformed section of the Jalhari granite is problematic, a phenomenon seen in numerous rocks of a variety of settings and ages (e.g., Proterozoic [Hawkins and Bowring 1997]; Paleozoic [Lanzirotti and Hanson 1996]; Mesozoic and Cenozoic [Parrish and Carr 1994]). Because accurate geochronologic assessment of monazite ages with respect to thermal histories is crucial to studies of tectonics in general, we discuss here possible interpretations of the monazite data. A number of primary and secondary processes can influence the age of monazite U-(Th)-Pb dates (e.g., xenocrystic inheritance, Pb-loss, hydrothermal growth, U-Th disequilibrium, deformation, etc.), but on the basis of the deformed nature of the Jalhari granite and local, abundant hot springs at Nanga Parbat, we are specifically concerned with how those processes impact our crystallization ages.

To lend some insight into fluid-mineral interaction, SEM-backscatter imaging was performed on the dated Jalhari granite monazites. Experimental and petrographic studies of monazite growth in-

dicated that patchy, complex zones grow from aqueous fluids (Hawkins and Bowring 1997; Teufel and Heinrich 1997; Ayers and Miller 1998), and, in our case, the grains showed chaotic and patchy replacement-related textures truncating magmatic zoning (e.g., concentric growth rims). In some cases, magmatic zoning was notably absent. In addition, the discrete, brighter backscatter zones within the monazite indicated higher U concentrations, which, when analyzed with the ion microprobe, tend to give younger Th-Pb ages. This is consistent with the positive correlation between Th-Pb age and the Th/U of the Jalhari monazite analyses (fig. 3). Geochronologic studies of rocks in the Himalaya and other orogens have shown that the U concentration can significantly influence Pb retentivity of accessory minerals (Parrish and Carr 1994). Minerals with very high U concentrations inevitably yield a spread of ages, with the actual crystallization date being the older ages within the spread. Cogenetic grains, which lose some component of their Pb* immediately following crystallization, will retain concordant U-(Th)-Pb compositions but will differ in age from neighboring grains depending on size and U concentration (Parrish and Carr 1994). The relatively high-U nature of the Jalhari granite monazites may have a direct effect on the Th-Pb age.

Deformation clearly must also play an important role in the crystallization history of monazites, although the effects are little studied. Teufel and Heinrich (1997) have investigated the effects of deformation on monazites through an experiment using monazite from a deformed rock. The monazite was powdered and placed in a high-temperature aqueous environment, which produced monazites with features recognized to be due to strong recrystallization and growth through a dissolution-precipitation mechanism. They demonstrated that during the dissolution-precipitation process, Pb is not incorporated into the newly grown monazites but remains in the fluid phase. In contrast, all of the U is reincorporated into the solid and no significant amounts of U are partitioned into the fluid. Subsequently, the Pb distribution within relict old and newly grown grains is inhomogeneous, resulting in a monazite system consisting of undisturbed monazite along with rejuvenated neoblastic monazite (Teufel and Heinrich 1997). This process is markedly different from Pb loss via hydrothermal leaching, which is limited to the surface of the grain (Teufel and Heinrich 1997).

In an environment of active deformation and abundant hot springs, it is easy to envisage a general dissolution-reprecipitation mechanism that is responsible for the spread of monazite ages in the Jalhari granite belt, which, in part, is incorporated into the Diamir shear zone. Independent isotopic studies suggest that fluid migration paths typically exploit the faults and shear zones at Nanga Parbat (Chamberlain et al. 1995; George and Bartlett 1996; Butler et al. 1997); we infer that hot fluids did vigorously circulate through the deforming Jalhari granite. Although no monazites were observed in thin section as part of our petrographic studies, it is apparent from the textures of other rock-forming minerals (e.g., feldspar) that there has been significant grain-boundary migration and wholesale grain-size reduction, suggesting conditions of deformation of >500°C for the Jalhari granite (Edwards et al. 2000). Moreover, the paucity of young zircons or zircon rims in the Jalhari granite from our three separate sample areas indicates that unlike granites at Tato (Zeitler et al. 1993) and Mazeno Pass (Schneider et al. 1999*c*), melting did not lead to precipitation of zircon rims. This could have resulted in excess zircon-derived U in the melt that became available for uptake into the reprecipitating monazite, resulting in high-U monazite with unreliably younger ages.

We propose initial intrusion of the Jalhari granite occurred at ~13 Ma, on the basis of the few monazite ages from the undeformed Garal section. Synchronous and subsequent ductile deformation within the Diamir section of the western NPHM margin, coupled with high-temperature fluid flow, is inferred to have produced dissolution and reprecipitation of monazites, probably well below the closure temperatures of Pb in monazites (>800°C) (Teufel and Heinrich 1997) but >500°C, on the basis of microstructures of the granite (Edwards et al. 2000). Ductile deformation of the exposed shear zone rocks ceased by 5–4 Ma, on the basis of cooling ages of the Diamir section (Winslow et al. 1996), hangingwall gneisses (this study), and the 6–4-Ma monazite ages from deformed gneisses along the Raikhot-Diamir shear zone (Jalipur augen gneiss [this study]; western Astor and Indus River gorges and Tato Valley [Smith et al. 1992]). Hot, U-rich fluids, however, after this time may have continued to circulate and reprecipitate monazite material on existing grains, in addition to possibly creating new, smaller monazites. This can explain our monazite dates that are younger than cooling ages and with low-Th/U (fig. 2).

In general, dissolution-precipitation and recrystallization mechanisms control the relative elemental retention among minerals that have been subjected to pervasive, postgrowth hydrothermal infiltration and deformation (Dahl 1997). These

mechanisms may easily produce disturbances and partial resetting of the U-(Th)-Pb isotope system in monazite, even at low temperatures of 400°C (Teufel and Heinrich 1997). Isotopic dating of ductile shear zones has been attempted in geochronologic studies of recrystallized minerals where extensive mass transfer occurs (Getty and Gromet 1992; Lanzirotti and Hanson 1995; George and Bartlett 1996; Lanzirotti and Hanson 1996; Resnor et al. 1996; Hawkins and Bowring 1997; Teufel and Heinrich 1997). However, because of the young and active nature of, and the large degree of reworking occurring within, the Diamir shear zone, it is only currently possible to constrain the age of the shear zone. We have succeeded in providing a transient "snapshot" of the deformation of the Jalhari granite and formation of the Diamir shear zone.

Implications

Geochronologic data from Nanga Parbat, amassed over the past decade, indicate a succession of tectonic processes responsible for the present configuration of the massif, and not a single late-stage event (fig. 8), punctuated by at least three tectonic episodes. Moreover, there appears to be a close spatial and temporal concordancy between metamorphic, magmatic, and cooling events inviting a model linking the association. We discuss these major tectonic events below.

Himalayan Collision. A few strong lines of evidence document initial or early stages of Himalayan collision at Nanga Parbat. Until recently the major features of the main Himalayan orogen at Nanga Parbat were believed to have been significantly overprinted by the most recent tectonic events or completely absent. U-Pb monazite ages from garnet inclusions and Sm-Nd garnet–whole-rock isotopic data indicate that garnet-grade metamorphic conditions were reached in the massif at ~44–36 Ma (Foster et al. 1999*b*, 2000); the Sm-Nd system records prograde metamorphic ages (Vance and Harris 1999). These Eocene ages are in agreement with other garnet–whole-rock, Sm-Nd and monazite inclusion ages for the northwest Himalaya (e.g., Garhwal Himalaya; Foster et al. 1999*b*, 2000). Perhaps more significantly, the presence of an ~19-Ma leucogranite pluton in southern Nanga Parbat (Schneider et al. 1999*b*) indicates that the Early Miocene anatexis, which is ubiquitous in central portions of the Himalaya (e.g., Harrison et al. 1997), did continue all the way to the western syntaxis. Furthermore, the cover sequence, particularly well-preserved in the southwestern corner of the massif, records cooling through ~300°C during the Oligocene (30–20 Ma). Cooling ages on other exposed Indian plate rocks of the northwest Himalaya are similar (e.g., Hazara syntaxis; Treloar and Rex 1990), indicating widespread "post-Himalayan" cooling. The Nanga Parbat massif clearly did experience, and in places still bears a record of, the effects of the early part of the Himalayan collision, which are recoverable with the advancement in reliable and precise geochronometers (fig. 8).

Late Miocene Metamorphism and Doming. Prior studies of Nanga Parbat have focused on the extremely young character of the massif, downplaying or overlooking the significance of "anomalously older" geochronologic data. Of note, however, and now relevant in view of our current data, is the fact that some Nanga Parbat studies have remarked upon older, but younger than Himalayan, metamorphic events. Winslow et al. (1996) suggested a metamorphic event at 12–10 Ma on the basis of SHRIMP depth-profiling of zircons from core gneisses of the massif. These zircons are characterized by distinct rims with low Th/U, typical for overgrowths. Smith et al. (1992) documented U-Pb monazite metamorphic ages as old as 11–9 Ma for gneisses in the Indus, Astor, and Tato Valleys, near the western margin, and concluded that the ages represent Neogene metamorphism. The Jutial pluton in the northwest corner of the massif yields concordant 9.5-Ma accessory mineral ages (Schneider et al. 1999*c*), and bedrock cooling ages from this area and elsewhere in the north are typically 12–5 Ma (e.g., George et al. 1995; George and Bartlett 1996; Reddy et al. 1997; Whittington 1997).

In light of these previous studies, the apparent complexity of our results is lessened and we are in a position to propose significant and detectable Late Miocene metamorphism and deformation within the massif. Th-Pb monazite ages on the undeformed Garal section of the Jalhari granite suggest that initial crystallization of this granite occurred at ~13 Ma; biotite cooling ages from the Airl Gali section of the Jalhari granite are similarly 13–10 Ma. In the southeast corner of the Nanga Parbat, adjacent to the Rupal shear, cooling ages are similar (≤15 Ma) and a crystallization age on a granite dike, which crosscuts the shear zone, is 9 Ma (Schneider et al. 1999*b*). Concordant Middle to Late Miocene U-Pb ages from the MMT dike (IK-05) may also record a melting event that produced zircon growth rims. These new data, combined with previous age data described above (Smith et al. 1992; Winslow et al. 1996; Schneider et al. 1999*c*), indicate a Late Miocene metamorphic, magmatic, and cooling signature that has been preserved within the massif (fig. 8).

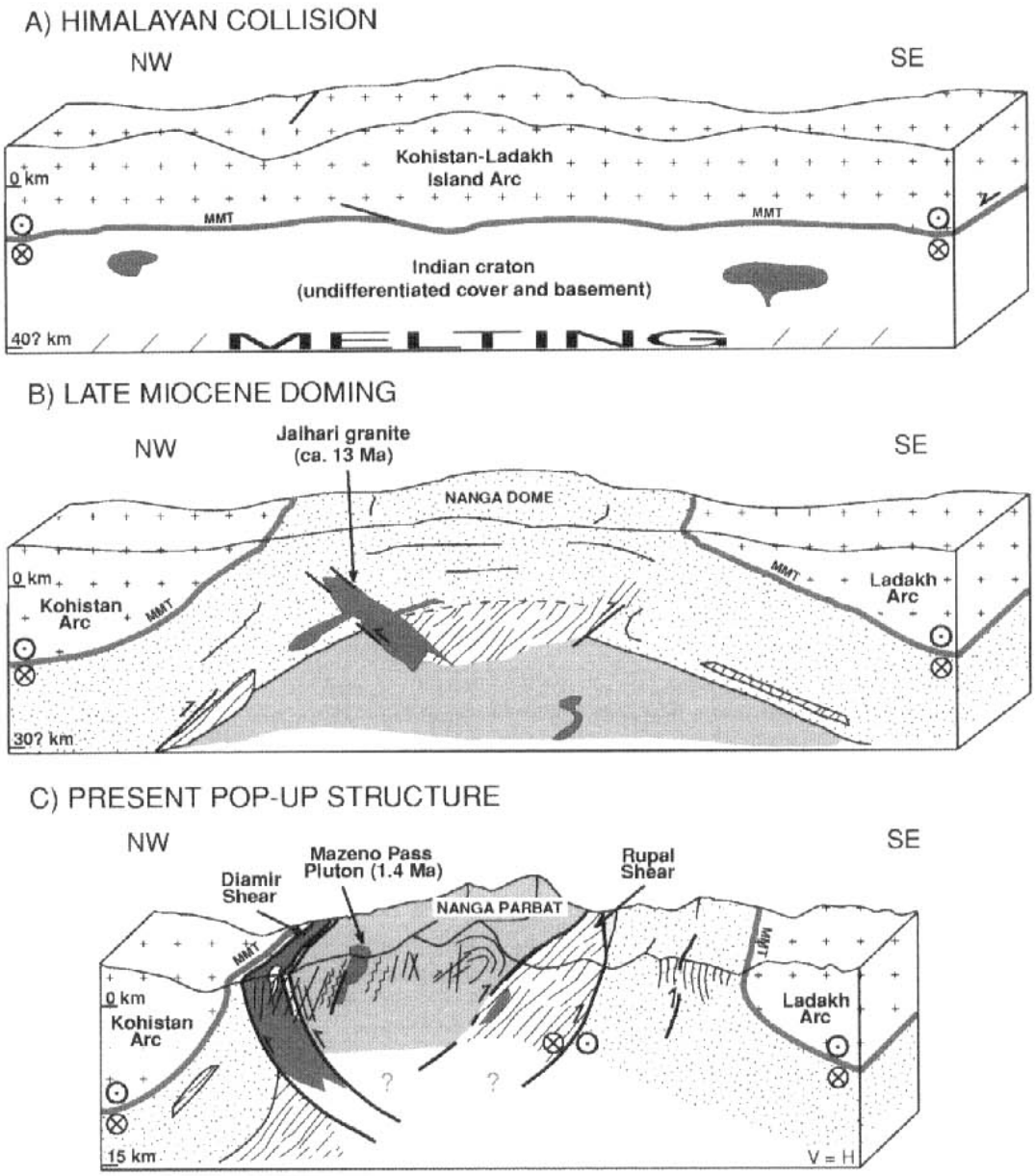

Figure 8. Himalayan evolution of Nanga Parbat since initial collision: *A*, overthrusting of Kohistan-Ladakh during early Himalayan collision leading to garnet growth and anatexis; *B*, Late Miocene doming, which affected the Himalaya-Karakorum region (Pêcher and Le Fort 1999) and is preserved at Haramosh and along the margins of Nanga Parbat; *C*, present-day pop-up structure (Schneider et al. 1999*a*). Geologic patterns are in figure 1. Note different scales.

In the northern portion of the massif, detailed mapping by Pêcher and Le Fort (1999) suggests that Haramosh is a large dome and a part of the southern Karakorum domes (Pêcher and Le Fort 1999) to the north and east. These domes are a series of Late Miocene dextral transpressional structures that developed along the Southern Karakorum fault, a reactivation of the Shyok suture (Pêcher and Le Fort 1999) and not to be confused with the Karakorum fault farther east. Regional deformation, accumulated through broad and diffuse northwest-southeast dextral-transpressive shearing within the Karakorum-Himalaya system, produced the observed pattern of a single corridor of east-west-trending domes. These structural domes yield Late Miocene mica and feldspar Ar-Ar cooling ages in the southern Karakorum (see Pêcher and Le Fort 1999 for complete thermochronologic references) and as far east as Indian Ladakh (Dunlap et al. 1998). This suggests that recent exhumation accompanied

doming in a crustal-scale fold system several hundreds of kilometers long.

In the southern portion of the massif, at Nanga Parbat proper, north-south rodding lineations mapped in the main river gorges (Edwards 1998; Butler et al. 2000) reflect constrictional finite strain as a consequence of distributed transpression (e.g., Fossen and Tikoff 1998). Butler et al. (2000) have suggested this as evidence for dextral shear combined with compression within the southern half of the massif. This is consistent with Seeber and Pêcher's (1998) regional model for the development of the massif.

Geochronologic results from across the massif discussed here, together with structural and isotopic evidence described in Pêcher and Le Fort (1999), are highly consistent with such a Late Miocene event affecting the entire massif. This is preserved at Haramosh but has been strongly overprinted by the Pliocene pop-up structure at Nanga Parbat. We concur with Pêcher and Le Fort (1999) that the Nanga Parbat massif underwent doming and metamorphism in the Late Miocene as a result of orogenic transpression, yielding to the protruding shape of the massif. There are no apparent domes to the west of Nanga Parbat, suggesting the Raikhot fault has accommodated significant amounts of transpression.

Pliocene and Younger Metamorphism and Deformation. The youngest portion of the Nanga Parbat massif is within the summit region, easily accessed from the Tato and Rupal Valleys. The geochronologic data that exist for this region consist of concordant young ages (<5 Ma) on numerous minerals (e.g., accessory minerals, micas) from various techniques (e.g., U-Pb, Th-Pb, Ar/Ar, fission track) with differing closure temperatures (>1000° to ~100°C). Spatial restriction of these core rocks, including granites, migmatites, and gneisses, to the pop-up structure of Nanga Parbat, and concordancy of young ages on those rocks, strongly suggest a close coupling of the very young (<5 Ma) metamorphic and deformational processes. Melting (via decompression?), concurrent with deformation and erosion-driven exhumation, has produced a pop-up structure with uplift occurring along the conjugate thrust pair crustal-scale shear zones. Timing constraints on structurally discordant dikes from the broad Rupal shear zone indicate that the outer portion of the shear zone may have been active at >10 Ma (Schneider et al. 1999*b*) and that deformation has migrated inward toward the center of the massif, on the basis of the young dikes' ages south of the summit presented in this study. We speculate that the original Rupal shear formed during Late Miocene doming of the area and has since continued to grow into the present width and form, suggesting a deformational continuum since the Late Miocene. Genesis of the Diamir shear probably likewise initiated during Late Miocene anatexis, on the basis of 13-Ma Jalhari granite ages. We suggest that the relatively hot granite provided a mechanical instability and became a locus of crustal weakness, thereby focusing the deformation that has resulted in the present Diamir shear zone. Localized melting likely further facilitated the deformation and enhanced the shear zone. We conclude that continued deformation rapidly uplifted the core zone rocks, resulting in the present pop-up structure (Schneider et al. 1999*a*), which overprinted the Late Miocene dome signature in southern Nanga Parbat (fig. 8). The deformation was possibly prompted by increased and efficient erosion along the western margin due to river capture of the Indus (Koons and Zeitler 1997; Zeitler et al. 2001) or arc parallel extension along the Himalaya (Seeber and Pêcher 1998). Erosion was not able to match uplift, creating great local relief and causing potential hydraulic head for circulating fluids (Craw et al. 1994). We infer that melting was promoted by the uplift of hot rock near the surface, significantly increasing the geothermal gradient (Winslow et al. 1994) whereby melting and deformation became part of a positive-feedback association (e.g., Hollister and Crawford 1986; Brown 1994). This activity, coupled with relentless erosion, resulted in rapid exhumation and cooling. This provides an explanation for the structural coincidence of the larger granites and shear zones and the chronologic coincidence of granite crystallization and bedrock cooling within the massif. The protracted uplift and associated exhumation would also explain the deep exposure of the Early Proterozoic basement of Lesser Himalaya affinity within the massif, flanked by cover sequence of Greater Himalaya affinity (Whittington et al. 1999).

Conclusions

Available evidence across the Nanga Parbat-Haramosh massif strongly suggests the massif is not purely the result of a single-stage tectonic event but is characterized by at least three tectonic events since initiation of Himalayan-collision, resulting in a dome-type structure modified in southern NPHM by a pop-up structure. The geologic and geochronologic relationships in the massif described above lead us to conclude the following: (1) The massif underwent metamorphism and deformation during general crustal thickening during the early stages

of the India-Asia collision, the result of which is preserved as Eocene to Early Miocene metamorphic and igneous ages in the core rocks and as Oligocene cooling of the cover sequences that flank the younger, high-grade core. (2) In the Late Miocene, transpression in the Himalaya-Karakorum syntaxial region resulted in a series of domes, subparallel to the Southern Karakorum fault, the thermal effects of which produced a second period of metamorphic and magmatic activity, preserved along the margins of the Nanga Parbat core rocks and throughout the Haramosh area. (3) Continuing deformation, accelerated since ~5 Ma and largely restricted to the southern half of the massif, produced granulite-grade metamorphism, anatectic melting, and rapid cooling with principal crustal displacement occurring via the pop-up mechanism.

This continuum of deformation and metamorphism indicates that the western syntaxis has undergone strong crustal reworking for a protracted length of time since the beginning of the Himalayan collision. The age patterns that we have defined show that the most recent activity is localized around what is now the summit region of Nanga Parbat; Late Miocene doming affected the entire NPHM and is certainly responsible for either the initiation of, or is a precursor to, the major conjugate thrust pair shear zone structures of the most recent event. The close spatial and temporal proximity of young granites and rapidly cooled high-grade rock suggests that there has been a positive-feedback process, with melting and deformation acting in concert with continued compression and erosion that has resulted in rapid uplift and exhumation of Nanga Parbat.

ACKNOWLEDGMENTS

This work was supported by U.S. National Science Foundation grants EAR 9418849 to P. Zeitler and EAR 9418730 to W. Kidd as part of the Nanga Parbat Continental Dynamics Project "Crustal Re-working During Orogeny." The ims 1270 Microprobe Facility at the University of California, Los Angeles, is supported in part by a grant from the National Science Foundation Instrument Facilities Program. Thanks to K. Repa (Material Sciences, Lehigh) for help with the SEM, R. Stern of the Geological Survey of Canada for supplying monazite standard 4170, and the National Center for Excellence–Geology, University of Peshawar, and numerous field assistants, guides, and porters in helping with fieldwork. B. Idleman and C. Coath assisted in the laboratory analyses. Discussions with A. Pêcher, P. Le Fort, G. Bebout, M. Harrison, and other members of the Nanga Parbat project are greatly appreciated. D. Holm, K. Hodges, C. Miller, and M. Searle provided comments on various versions of the manuscript.

REFERENCES CITED

Amato, J. M.; Wright, J. E.; Gans, P. B.; and Miller, E. L. 1994. Magmatically induced metamorphism and deformation in the Kigluaik gneiss dome, Seward Peninsula, Alaska. Tectonics 13:515–527.

Ayers, J. C., and Miller, C. F. 1998. How do monazite and zircon grow, and what do monazite and zircon U-Pb age dates mean? insights obtained from experiments. Geol. Soc. Am. Abstr. 30:A214.

Baldwin, S.; Lister, G.; Hill, E.; Foster, D.; and McDougall, I. 1993. Thermochronologic constraints on the tectonic evolution of active metamorphic core complexes, D'entrecasteaux Island, Papua New Guinea. Tectonics 12:611–628.

Barth, S.; Oberli F.; and Meier, M. 1989. U-Th-Pb systematics of morphologically characterized zircon and allanite: a high resolution isotopic study of the Alpine Rensen pluton (northern Italy). Earth Planet. Sci. Lett. 95:235–254.

Brown, M. 1994. The generation, segregation, ascent and emplacement of granite magma: the migmatite-to-crustally-derived granite connection in thickened orogens. Earth Sci. Rev. 36:83–130.

Burbank, D.; Leland, J.; Fielding, E.; Anderson, R.; Brozovic, N.; Reid, M.; and Duncan, C. 1996. Bedrock incision, rock uplift and threshold hillslopes in the northwest Himalayas. Nature 364:48–50.

Butler, R.; Harris, N.; and Whittington, A. 1997. Interactions between deformation, magmatism, and hydrothermal activity during crustal thickening: a field example from Nanga Parbat, Pakistan Himalaya. Mineral. Mag. 61:37–51.

Butler, R.; Wheeler, J.; Treloar, P.; and Jones, C. 2000. Geologic structure of the southern part of the Nanga Parbat massif, Pakistan, and its tectonic implications. *In* Khan, A.; Searle, M.; and Treloar, P., eds. Tectonics of the Nanga Parbat syntaxis and the western Himalaya. Geol. Soc. Lond. Spec. Pub. 170:123–136.

Chamberlain C. P.; Zeitler, P. K.; Barnett, D.; Winslow, D.; Poulson, S.; Leahy, T.; and Hammer, J. 1995. Active hydrothermal systems during the recent uplift of Nanga Parbat, Pakistan Himalaya. J. Geophys. Res. 100:439–453.

Chamberlain, C. P.; Zeitler, P. K.; and Erickson, E. 1991. Constraints on the tectonic evolution of the north-

west Himalaya from geochronologic and petrologic studies of Babusar Pass, Pakistan. J. Geol. 99:829–849.

Craw, D.; Koons, P. O.; Winslow, D.; Chamberlain, C. P.; and Zeitler, P. K. 1994. Boiling fluids in a region of rapid uplift, Nanga Parbat massif, Pakistan. Earth Planet. Sci. Lett. 128:169–182.

Dahl, P. S. 1997. A crystal-chemical basis for Pb retention and fission-track annealing systematics in U-bearing minerals, with implications for geochronology. Earth Planet. Sci. Lett. 150:277–290.

Dunlap, W. J.; Weinberg, R.; and Searle, M. 1998. Karakorum fault zone rocks cool in two phases. J. Geol. Soc. Lond. 155:903–912.

Edwards, M. A. 1998. Examples of tectonic mechanisms for local contraction and exhumation of the leading edge of India, southern Tibet and Nanga Parbat, Pakistan. Ph.D. thesis, State University of New York, Albany.

Edwards, M. A.; Kidd, W. S. F.; Khan, M. A.; and Schneider, D. A. 2000. Tectonics of the SW margin of Nanga Parbat-Haramosh Massif. *In* Khan, A.; Searle, M.; and Treloar, P., eds. Tectonics of the Nanga Parbat syntaxis and the western Himalaya. Geol. Soc. Lond. Spec. Pub. 170:200–217.

Fossen, H., and Tikoff, B. 1998. Extended models of transpression and transtension, and application to tectonic settings. *In* Holdsworth, M.; Dewey, J.; and Strachan, R., eds. Continental transpression and transtension tectonics. Geol. Soc. Lond. Spec. Pub. 135:15–33.

Foster, G.; Kinny, P.; Vance, D.; Harris, N.; Argles, T.; and Whittington, A. 1999*a*. The Pre-Tertiary metamorphic history of the Nanga Parbat Haramosh massif, Pakistan Himalaya. Himalayan-Karakorum-Tibetan Workshop Abstr. 14:44–45.

Foster, G.; Kinny, P.; Vance, D.; Prince, C.; and Harris, N. 2000. The significance of monazite U-Th-Pb age data in metamorphic assemblages; a combined study of monazite and garnet chronometry. Earth Planet. Sci. Lett. 181:327–340.

Foster, G.; Vance, D.; Prince, C.; and Harris, N. 1999*b*. Along-arc variations in the time scales of Himalayan prograde metamorphism and anatexis. Eur. Union Geophys. 10:131.

George, M., and Bartlett, J. 1996. Rejuvenation of Rb-Sr mica ages during shearing on the northwestern margin of the Nanga Parbat-Haramosh massif. Tectonophysics 260:167–185.

George, M.; Reddy, S.; and Harris, N. 1995. Isotopic constraints on the cooling history of the Nanga Parbat-Haramosh massif and Kohistan arc, western Himalaya. Tectonics 14:237–252.

Getty, S., and Gromet, P. 1992. Geochronological constraints on ductile deformation, crustal extension, and doming about a basement-cover boundary, New England Appalachians. Am. J. Sci. 292:359–397.

Harrison, T. M.; Grove, M.; McKeegan, K.; Coath, C.; Lovera, O.; and Le Fort, P. 1999. Origin and episodic emplacement of the Manaslu Intrusive Complex, central Himalaya. J. Petrol. 40:3–19.

Harrison, T. M.; Lovera, O.; and Grove, M. 1997. New insights into the origin of two contrasting Himalayan granite belts. Geology 25:899–902.

Hawkins, D., and Bowring, S. 1997. U-Pb systematics of monazite and xenotime: case studies from Paleoproterozoic of the Grand Canyon, Arizona. Contrib. Mineral. Petrol. 127:87–103.

Hollister, L., and Crawford, K. 1986. Melt-enhanced deformation: a major tectonic process. Geology 14: 558–561.

Koons, P. O., and Zeitler, P. K. 1997. Himalayan tectonics with a grain of salt: a view from the left-hand edge. EOS: Trans. Am. Geophys. Union 78:S111.

Lanzirotti, A., and Hanson, G. 1995. U-Pb dating of major and accessory minerals formed during metamorphism and deformation of metapelites. Geochim. Cosmochim. Acta 59:2513–2526.

———. 1996. Geochronology and geochemistry of multiple generations of monazite from the Wewapaug Schist, CT, USA, implications for monazite stability in metamorphic rocks. Contrib. Mineral. Petrol. 125: 332–340.

Le Fort, P.; Debon, F.; Pêcher, A.; Sonet, J.; and Vidal, P. 1986. The 500 Ma magmatic event in Alpine southern Asia, a thermal episode at Gondwana scale. Sci. Terre 47:191–209.

Madin, I. P.; Lawrence, R. D.; and Ur-Rehman, S. 1989. The northwestern Nanga Parbat massif: evidence for crustal uplift at the northwestern corner of the Indian craton. *In* Malinconico, L. L., and Lillie, R. J., eds. Tectonics of the western Himalayas. Boulder, Colo., Geol. Soc. Am. Spec. Pap. 232:169–182.

Parrish, R., and Carr, S. 1994. U-Pb problematics of very high-U accessory minerals: examples from the Himalaya and Cordillera and implications for U-Pb geochronology. ICOG Abstr. 8:243.

Pêcher, A., and Le Fort, P. 1999. Late Miocene tectonic evolution of the Karakorum-Nanga Parbat contact zone (northern Pakistan). *In* Macfarlane, A.; Qude, J.; and Sorkhabi, R., eds. Himalaya and Tibet: mountain roots to mountain tops. Boulder, Colo., Geol. Soc. Am. Spec. Pap. 328:145–158.

Poage, M. A.; Chamberlain, C. P.; and Craw, D. 2000. Massif-wide metamorphism and fluid evolution at Nanga Parbat, northern Pakistan. Am. J. Sci. 300: 463–482.

Reddy, S.; Kelley, S.; and Magennis, L. 1997. A microstructural and argon laserprobe study of shearzone development at the western margin of the Nanga Parbat-Haramosh Massif, western Himalaya. Contrib. Mineral. Petrol. 128:16–29.

Resnor, P.; Chamberlain, K.; Frost, C.; Snoke, A.; and Frost, B. R. 1996. Direct dating of deformation: U-Pb age of syndeformational sphene growth in the Proterozoic Laramie Peak shear zone. Geology 24:623–626.

Schneider, D. A.; Edwards, M. A.; Kidd, W. S. F.; Khan, M. A.; Seeber, L.; and Zeitler, P. K. 1999*a*. Tectonics of Nanga Parbat, western Himalaya: synkinematic plutonism within the doubly vergent shear zones of a crustal-scale pop-up structure. Geology 27:999–1002.

Schneider, D. A.; Edwards, M. A.; Kidd, W. S. F.; Zeitler,

P. K.; and Coath, C. 1999*b*. Early Miocene anatexis identified in the western syntaxis, Pakistan Himalaya. Earth Planet. Sci. Lett. 167:121–129.

Schneider, D. A.; Edwards, M. A.; Zeitler, P. K.; and Coath, C. 1999*c*. Mazeno Pass Pluton and Jutial Granite, Pakistan Himalaya: age and implications for entrapment mechanisms of two granites in the Himalaya. Contrib. Mineral. Petrol. 136:273–284.

Schneider, D. A.; Zeitler, P. K.; Edwards, M. A.; and Kidd, W. S. F. 1997. Geochronologic constraints on the geometry and timing of anatexis and exhumation at Nanga Parbat: a progress report. EOS: Trans. Am. Geophys. Union 78:S111.

Seeber, L., and Pêcher, A. 1998. Strain partitioning along the Himalayan arc and the Nanga Parbat antiform. Geology 26:791–794.

Shroder, J., and Bishop, M. 1999. Monsoon linkages to western Himalaya denudation and tectonics. Geol. Soc. Am. Abstr. 31:A141.

Smith, H. A.; Chamberlain, C. P.; and Zeitler, P. K. 1992. Documentation of Neogene regional metamorphism in the Himalayas of Pakistan using U-Pb in monazite. Earth Planet. Sci. Lett. 113:93–105.

———. 1994. Timing and duration of Himalayan metamorphism within the Indian plate, northwest Himalaya, Pakistan. J. Geol. 102:493–508.

Stanfill, A. 1997. Implications of intrusive igneous dikes on the thermochronologic ages of micas, Nanga Parbat-Haramosh massif, Pakistan. Senior thesis, Lehigh University, Bethlehem, Pa.

Teufel, S., and Heinrich, W. 1997. Partial resetting of the U-Pb isotope system in monazite through hydrothermal experiments: an SEM and U-Pb isotope study. Chem. Geol. 137:273–281.

Treloar, P. J.; Potts, G. J.; Wheeler, J.; and Rex, D. C. 1991. Structural evolution and asymmetric uplift of the Nanga Parbat syntaxis, Pakistan Himalaya. Geol. Rundsch. 80:411–428.

Treloar, P. J., and Rex, D. 1990. Cooling and uplift histories of the crystalline thrust stack of the Indian Plate internal zones west of Nanga Parbat, Pakistan Himalaya. Tectonophysics 180:323–349.

Treloar, P. J.; Rex, D.; Guise, P.; Coward, M.; Searle, M.; Petterson, M.; Windley, B.; Jan, M. Q.; and Luff, I. 1989. K-Ar and Ar-Ar geochronology of the Himalayan collision in NW Pakistan: constraints on the timing of collision, deformation, metamorphism, and uplift. Tectonics 8:881–909.

Treloar, P. J.; Rex, D.; Guise, P.; Wheeler, J.; Hurford, A.; and Carter, A. 2000. Geochronologic constraints on the evolution of the Nanga Parbat syntaxis, Pakistan Himalaya. *In* Khan, A.; Searle, M.; and Treloar, P., eds. Tectonics of the Nanga Parbat syntaxis and the western Himalaya. Geol. Soc. Lond. Spec. Pub. 170: 137–162.

Vance, D., and Harris, N. 1999. Timing of prograde metamorphism in the Zanskar Himalaya. Geology 27: 395–398.

Whittington, A. 1997. The thermal, metamorphic and magmatic evolution of a rapidly exhuming terrane: the Nanga Parbat Massif, northern Pakistan. Ph.D. thesis, Open University, Milton Keynes, U.K.

Whittington, A.; Foster, G.; Harris, N.; Vance, D.; and Ayres, M. 1999. Lithostratigraphic correlations in the western Himalaya—an isotopic approach. Geology 27: 585–588.

Winslow, D. M.; Zeitler, P. K.; and Chamberlain, C. P. 1994. Direct evidence for a steep geotherm under conditions of rapid denudation, western Himalaya, Pakistan. Geology 22:1075–1078.

Winslow, D. M.; Zeitler, P. K.; Chamberlain, C. P.; and Williams, I. S. 1996. Geochronologic constraints on syntaxial development in the NPHM, Pakistan. Tectonics 15:1292–1308.

Zeitler, P. K. 1985. Cooling history of the NW Himalaya, Pakistan. Tectonics 4:127–151.

Zeitler, P. K., and Chamberlain, C. P. 1991. Petrogenetic and tectonic significance of young leucogranites from the NW Himalaya, Pakistan. Tectonics 10:729–741.

Zeitler, P. K.; Chamberlain, C. P.; and Smith, H. A. 1993. Synchronous anatexis, metamorphism, and rapid denudation at Nanga Parbat, Pakistan Himalaya. Geology 21:347–350.

Zeitler, P. K.; Sutter, J.; Williams, I. S.; Zartman, R. E.; and Tahirkheli, R. A. K. 1989. Geochronology and temperature history of the NPHM, Pakistan. *In* Malinconico, L. L., and Lillie, R. J., eds. Tectonics of the Western Himalayas. Boulder, Colo., Geol. Soc. Am. Spec. Pap. 232:1–23.

Zeitler, P. K., and the Nanga Parbat Working Group. 2001. Erosion, Himalayan geodynamics, and the geomorphology of metamorphism. GSA Today 11:4–9.